Ⓔ

TIME-RESOLVED PHOTOMETRY OF KUIPER BELT OBJECTS: ROTATIONS, SHAPES, AND PHASE FUNCTIONS

SCOTT S. SHEPPARD AND DAVID C. JEWITT
Institute for Astronomy, University of Hawaii, 2680 Woodlawn Drive, Honolulu, HI 96822;
sheppard@ifa.hawaii.edu, jewitt@ifa.hawaii.edu

ABSTRACT

We present a systematic investigation of the rotational light curves of trans-Neptunian objects based on extensive optical data from Mauna Kea. Four of 13 objects (corresponding to 31%) in our sample [(33128) 1998 BU_{48}, 2000 GN_{171}, (20000) Varuna, and (40314) 1999 KR_{16}] were found to exhibit light curves with peak-to-peak range ≥0.15 mag. In a larger sample obtained by combining our data with reliably determined light curves from the literature, seven of 22 objects (32%) display significant (≥0.15 mag range) light curves. About 23% of the sampled objects have light-curve ranges ≥0.4 mag. Curiously, the objects are very large ($\gtrsim 250$ km diameter, assuming an albedo of 0.04) and, in the absence of rotation, should be nearly spherical as a result of self-compression. We propose that the large-amplitude, short-period objects are rotationally distorted, low-density rubble piles. Statistically, the trans-Neptunian objects are less spherical than their main-belt asteroid counterparts, indicating a higher specific angular momentum, perhaps resulting from the formation epoch. In addition to the rotational light curves, we measured phase darkening for seven Kuiper belt objects in the $0°$ to $2°$ phase-angle range. Unlike Pluto, the measured values show steep slopes and moderate opposition surge, indicating backscatter from low-albedo porous surface materials.

Key words: Kuiper belt — minor planets, asteroids — Oort cloud — solar system: general

On-line material: machine-readable table

1. INTRODUCTION

More than 500 trans-Neptunian objects (TNOs) have been discovered in the decade since the discovery of 1992 QB_1 (Jewitt & Luu 1993). These objects make up the Kuiper belt (also known as the Edgeworth-Kuiper belt), which is thought to contain about 70,000 objects with radii greater than 50 km (Jewitt, Luu, & Chen 1996). The Kuiper belt is thought to be a relic from the original protoplanetary disk, albeit one that has been dynamically disturbed and collisionally processed in ways that are not yet fully understood.

The Kuiper belt is the most likely source of the Jupiter-family comets (Fernández 1980; Duncan, Quinn, & Tremaine 1988). It is by far the largest long-lived reservoir of small bodies in the planetary region, outnumbering the main-belt asteroids and Jovian Trojans by a factor of ~300. The Kuiper belt objects (KBOs) are further thought to be chemically primitive, containing trapped volatiles and having experienced relatively little thermal evolution since formation. Thus, we may be able to probe some aspects of the early history of the local solar nebula by studying the Kuiper belt and related objects.

The determination of the physical characteristics of the KBOs has proceeded very slowly. This is because even the brightest known KBOs (other than Pluto and Charon) only reach apparent red magnitude $m_R \sim 19.5$ and thus are challenging target with current spectroscopic technology. The surfaces of KBOs may have been altered over their lifetimes by collisions, cometary activity, and irradiation. The largest KBOs might even be partially differentiated as a result of radiogenic heating. This could lead to the spinning up of objects to conserve angular momentum. Colors of the KBOs have been found to be diverse, ranging from neutral to very red ($V-R \sim 0.3$ to $V-R \sim 0.8$; Luu & Jewitt 1996; Green et al. 1997; Tegler & Romanishin 2000; Jewitt & Luu

2001). While spectra of KBOs are mostly featureless, some show weak 2 μm water ice absorptions (Brown, Cruikshank, & Pendleton 1999; Jewitt & Luu 2001). Most KBOs are too distant ($\gtrsim 30$ AU) and small to resolve with current technology. They are also very cold objects (~50 K) that emit most of their thermal radiation in the inaccessible far-infrared wavelengths, requiring observations from above Earth's atmosphere. Thus, the most feasible way to determine KBOs shapes and surface features is through their photometric light variations.

The rotations and shapes of the KBOs may be a function of their size. Small KBOs (diameters $D < 100$ km) are thought to be collisionally produced (Farinella & Davis 1996). These objects retain no memory of the primordial angular momentum of their parent bodies. Instead, their spins are presumably set by the partitioning of kinetic energy delivered by the projectile responsible for breakup. Larger objects may be structurally damaged bodies held together by gravity (rubble piles; Jewitt & Sheppard 2002). The spins of these objects should be much less influenced by recent impacts. A similar situation prevails in the main asteroid belt, where collisional modification of the rotations and shapes of the smaller objects is observationally well established (Catullo et al. 1984). The large objects in both the main belt and the Kuiper belt may provide a record of the primordial distribution of angular momenta imbued by the growth process. A key attribute of the Kuiper belt is that the population is very large compared with the main asteroid belt, allowing access to a substantial sample of objects that are too large to have been influenced by recent collisions.

We here use voluminous time-resolved photometric observations to determine the rotational light curves, colors, and phase functions of KBOs. As our sample, we select the intrinsically brightest (presumably largest) KBOs.

Specifically, we observed KBOs having absolute magnitude $H_R \leq 7.5$, corresponding to $D \geq 200$ km if a red geometric albedo of $p_R = 0.04$ is assumed. We use most of the known KBOs with $H_R \leq 6.0$, which corresponds to $D \geq 375$ km in our analysis. The objects observed were all bright, in order to guarantee high signal-to-noise ratios in short exposures to adequately sample the KBO light curves.

2. OBSERVATIONS

The University of Hawaii 2.2 m diameter telescope atop Mauna Kea, in Hawaii, was used with a 2048×2048 pixel Tektronix CCD (24 μm pixels) and a $0\rlap{.}''219$ pixel^{-1} scale at the f/10 Cassegrain focus. An antireflection coating provides very high average quantum efficiency (0.90) in the R band. The field of view was $7\rlap{.}'5 \times 7\rlap{.}'5$. Exposures were taken using $BVRI$ filters based on the Johnson-Kron-Cousins system, while the telescope was autoguided on bright nearby stars. The seeing ranged from $0\rlap{.}''6$ to $1\rlap{.}''5$ during the many nights of observation throughout 1999, 2000, and 2001. Objects moved relative to the fixed stars at a maximum of $4''$ hr^{-1}, corresponding to trail lengths $\leq 0\rlap{.}''45$ in the longest (400 s) exposures. Even for the fastest-moving objects in the longest exposures, the trailing motion is small compared with the seeing and so can be neglected as a source of error in the photometry.

The images were bias-subtracted and then flat-fielded using the median of a set of dithered images of the twilight sky. Landolt (1992) standard stars were used for the absolute photometric calibration. Photometry of faint objects, such as the KBOs, must be done very carefully to achieve accurate results. To optimize the signal-to-noise ratio, we performed aperture correction photometry by using a small aperture on the KBOs ($0\rlap{.}''65–0\rlap{.}''88$ in radius) and both the same small aperture and a large aperture ($2\rlap{.}''40–3\rlap{.}''29$ in radius) on (four or more) nearby bright field stars. We corrected the magnitude within the small aperture used for the KBOs by determining the correction from the small to the large aperture using the field stars (cf. Tegler & Romanishin 2000; Jewitt & Luu 2001). Since the KBOs moved slowly, we were able to use the same field stars from night to night within each observing run. Thus, relative photometric calibration from night to night was very constant. The few observations that were taken in mildly nonphotometric conditions were calibrated to observations of the same field stars on the photometric nights. The observational circumstances, geometry, and orbital characteristics of the 13 observed KBOs are shown in Tables 1 and 2, respectively.

3. LIGHT-CURVE RESULTS

The photometric results for the 13 KBOs are listed in Table 3, where the columns include the start time of each integration, the corresponding Julian Date, and the magnitude. No correction for light-travel time has been made. Results of the light-curve analysis for all the KBOs observed are summarized in Table 4, while the mean colors can be found in Table 5. We first discuss the light curves of (20000) Varuna, 2000 GN$_{171}$, (33128) 1998 BU$_{48}$, and (40314) 1999 KR$_{16}$ and give some details about the null results below.

We employed the phase dispersion minimization (PDM) method (Stellingwerf 1978) to search for periodicity in the data. In PDM, the metric is the so-called Θ-parameter, which is essentially the variance of the data when phased by

TABLE 1
GEOMETRIC CIRCUMSTANCES OF THE OBSERVATIONS

UT Date	R (AU)	Δ (AU)	α (deg)
(38628) 2000 EB$_{173}$:			
2001 Feb 21	29.77	29.12	1.45
2001 Apr 21	29.75	28.77	0.47
2001 Apr 22	29.74	28.77	0.49
2001 Jun 30	29.71	29.52	1.93
(26375) 1999 DE$_9$:			
2000 Apr 28	33.79	33.36	1.55
2000 Apr 30	33.79	33.39	1.58
2000 May 1	33.79	33.40	1.59
2001 Feb 19	33.96	32.98	0.18
2001 Feb 21	33.96	32.97	0.12
2001 Apr 24	34.00	33.47	1.45
2001 Apr 25	34.00	33.49	1.47
(26181) 1996 GQ$_{21}$:			
2001 Feb 21	39.25	38.75	1.26
2001 Apr 20	39.28	38.27	0.12
2001 Apr 21	39.28	38.27	0.11
2001 Apr 22	39.28	38.27	0.11
2001 Apr 23	39.28	38.28	0.11
2001 Apr 25	39.28	38.28	0.14
2000 GN$_{171}$:			
2001 Apr 20	28.80	27.82	0.44
2001 Apr 21	28.80	27.82	0.48
2001 Apr 22	28.80	27.83	0.51
2001 Apr 23	28.80	27.83	0.54
2001 Apr 24	28.80	27.84	0.58
2001 Apr 25	28.80	27.84	0.61
2001 May 11	28.79	27.95	1.11
2001 May 12	28.79	27.96	1.14
2001 May 13	28.79	27.97	1.17
(19521) Chaos 1998 WH$_{24}$:			
1999 Nov 9	42.39	41.42	0.28
1999 Nov 10	42.39	41.42	0.26
(33340) 1998 VG$_{44}$:			
1999 Nov 11	30.46	29.49	0.32
1999 Nov 12	30.46	29.48	0.29
2001 FZ$_{173}$:			
2001 Apr 24	33.23	32.42	1.04
2001 Apr 25	33.23	32.43	1.06
(33128) 1998 BU$_{48}$:			
2001 Feb 21	27.60	26.64	0.45
2001 Apr 25	27.68	27.42	2.02
2001 Nov 14	27.93	27.96	2.03
2001 Nov 16	27.94	27.92	2.03
2001 Nov 17	27.94	27.91	2.03
2001 Nov 18	27.94	27.89	2.03
2001 Nov 19	27.94	27.88	2.03
(40314) 1999 KR$_{16}$:			
2000 Apr 28	38.04	37.05	0.31
2000 Apr 30	38.03	37.05	0.36
2000 May 1	38.03	37.06	0.38
2001 Feb 18	37.84	37.33	1.30
2001 Feb 19	37.84	37.32	1.28
2001 Apr 24	37.80	36.80	0.16
2001 Apr 25	37.80	36.80	0.18
2001 May 11	37.80	36.86	0.59
2001 May 12	37.79	36.86	0.62
2001 May 13	37.79	36.87	0.64
1997 CS$_{29}$:			
2001 Feb 21	43.59	42.77	0.73
2001 CZ$_{31}$:			
2001 Feb 20	41.41	40.47	0.44
2001 Feb 21	41.41	40.48	0.46
2001 Apr 20	41.41	41.19	1.36
1998 HK$_{151}$:			
2001 May 1	30.38	29.40	0.46
2001 May 2	30.38	29.40	0.43

TABLE 2
PARAMETERS OF OBSERVED OBJECTS

Object		Class[a]	H (mag)	i (deg)	e	a (AU)
(38628)	2000 EB$_{173}$	R	4.7	15.5	0.273	39.3
(20000) Varuna	2000 WR$_{106}$	C	3.7	17.1	0.055	43.2
(26375)	1999 DE$_9$	S	4.7	7.6	0.423	55.9
(26181)	1996 GQ$_{21}$	S	5.2	13.4	0.588	92.8
	2000 GN$_{171}$	R	5.8	10.8	0.279	39.3
(19521) Chaos	1998 WH$_{24}$	C	4.9	12.0	0.110	46.1
(33340)	1998 VG$_{44}$	R	6.5	3.0	0.260	39.6
	2001 FZ$_{173}$	S	6.2	12.2	0.622	88.0
(33128)	1998 BU$_{48}$	S	7.2	14.2	0.387	33.5
(40314)	1999 KR$_{16}$	C	5.8	24.9	0.298	48.5
	1997 CS$_{29}$	C	5.2	2.2	0.015	44.2
	2001 CZ$_{31}$	C	5.5	10.2	0.097	45.3
	1998 HK$_{151}$	R	7.6	6.0	0.224	39.1

NOTE.—Parameters are from the Minor Planet Center. H is the absolute magnitude, which is the object's brightness if it were at 1 AU from the Sun and Earth and the phase angle were zero, i is the inclination, e is the eccentricity, and a is the semi major axis.

[a] (S) Scattered-type object; (C) classical-type object; (R) resonance-type object.

a given period divided by the variance of the unphased data. The best-fit period should have a very small dispersion compared with the unphased data, and thus $\Theta \ll 1$ indicates that a good fit has been found.

3.1. (20000) Varuna

Varuna shows a large, periodic photometric variation (Farnham 2001). We measured a range $\Delta m_R = 0.42 \pm 0.02$ mag and best-fit, two-peaked light-curve period $P = 6.3436 \pm 0.0002$ hr (about twice the period reported by Farnham), with no evidence for a rotational modulation in the $B-V$, $V-R$, or $R-I$ color index. These results, and their interpretation in terms of a rotating, elongated rubble pile of low bulk density, are described in detail in Jewitt & Sheppard (2002).

3.2. 2000 GN$_{171}$

PDM analysis shows that 2000 GN$_{171}$ has strong PDM minima near periods $P = 4.17$ hr and $P = 8.33$ hr, with weaker 24 hr alias periods flanking each of these (Fig. 1).
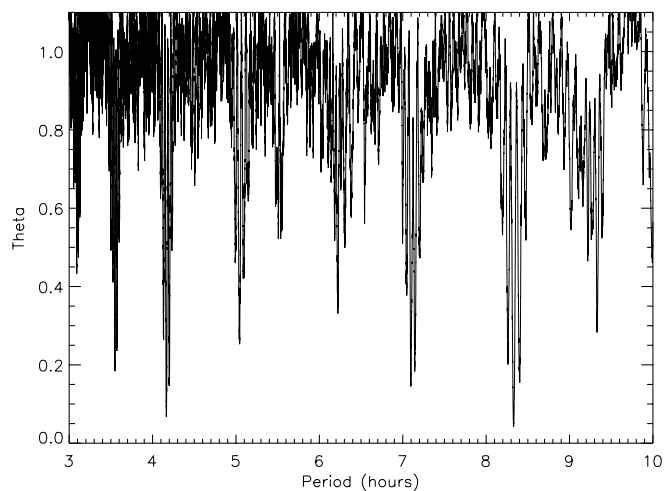

FIG. 1.—Phase dispersion minimization plot for 2000 GN$_{171}$. A smaller θ corresponds to a better fit. Best fits from this plot are the 4.12 hr single-peaked fit and the 8.32 hr double-peaked fit. Both are flanked by 24 hr alias periods.

We phased the data to all the peaks with $\Theta < 0.4$ and found only the 4.17 and 8.33 hr periods to be consistent with all the data. The $P = 4.17$ hr period gives a light curve with a single maximum per period, while the $P = 8.33$ hr light curve has two maxima per period, as expected for rotational modulation caused by an aspherical shape. Through visual inspection of the phased light curves, we find that the phase plot for $P = 4.17$ hr (Fig. 2) is more scattered than that for the longer period of $P = 8.33$ hr (Fig. 3). This is because the double-peaked phase plot shows a significant asymmetry of $\Delta \sim 0.08$ mag between the two upper and lower peaks. A closer view of the PDM plot in Figure 4 around the double-peaked period allows us to obtain a rotation period of $P_{\rm rot} = 8.329 \pm 0.005$ hr with a peak-to-peak variation of $\Delta m = 0.61 \pm 0.03$ mag. We believe that the photometric variations in 2000 GN$_{171}$ are due to its elongated shape rather than to albedo variations on its surface.

Broadband $BVRI$ colors of 2000 GN$_{171}$ show no variation throughout its rotation within the photometric uncertainties of a few percent (Figs. 5 and 6 and Table 6). This again suggests that the light curve is mostly caused by an elongated object with a nearly uniform surface. The colors

TABLE 3
OBSERVATIONS OF KUIPER BELT OBJECTS

Object	Image[a]	UT Date[b]	Julian Date[c]	Exp.[d] (s)	Mag.[e] (m_R)
(38628) 2000 EB$_{173}$	6066	2001 Feb 21.4853	2,451,961.9853	200	19.318
	6067	2001 Feb 21.4889	2,451,961.9889	200	19.323
	6072	2001 Feb 21.5195	2,451,962.0195	200	19.360
	6073	2001 Feb 21.5231	2,451,962.0231	200	19.363
	6081	2001 Feb 21.5658	2,451,962.0658	200	19.364

NOTE.—Table 3 is presented in its entirety in the electronic edition of the Astronomical Journal. A portion is shown here for guidance regarding its form and content.

[a] Image number.
[b] Decimal Universal Date at the start of the integration.
[c] Julian Date at the start of the integration.
[d] Exposure time for the image.
[e] Apparent red magnitude; uncertainties are ± 0.02–0.03 for the brighter objects (<21.0 mag) and ± 0.04–0.05 for fainter objects.

TABLE 4
Properties of Observed KBOs

Object		m_R[a] (mag)	Nights[b]	Δm_R[c] (mag)	Single[d] (hr)	Double[e] (hr)
(38628)	2000 EB$_{173}$	19.18 ± 0.03	3	<0.06	...	...
(20000) Varuna	2000 WR$_{106}$[f]	19.70 ± 0.25	8	0.42 ± 0.03	...	6.34 ± 0.01
(26375)	1999 DE$_9$...........	20.02 ± 0.03	3	<0.10	>12?	...
(26181)	1996 GQ$_{21}$	20.35 ± 0.04	6	<0.10	...	...
	2000 GN$_{171}$	20.60 ± 0.30	9	0.61 ± 0.03	...	8.329 ± 0.005
(19521) Chaos	1998 WH$_{24}$	20.65 ± 0.10	2	<0.10	?	?
(33340)	1998 VG$_{44}$	20.95 ± 0.10	3	<0.10	...	...
	2001 FZ$_{173}$	21.05 ± 0.05	2	<0.06	...	...
(33128)	1998 BU$_{48}$	21.25 ± 0.35	7	0.68 ± 0.04	4.9 ± 0.1	9.8 ± 0.1
					6.3 ± 0.1	12.6 ± 0.1
(40314)	1999 KR$_{16}$........	21.15 ± 0.15	10	0.18 ± 0.04	5.929 ± 0.001	11.858 ± 0.002
					5.840 ± 0.001	11.680 ± 0.002
	1997 CS$_{29}$	21.36 ± 0.04	1	<0.08	...	...
	2001 CZ$_{31}$..........	21.70 ± 0.10	5	<0.20	?	?
	1998 HK$_{151}$	21.75 ± 0.05	2	<0.15	...	...

[a] Mean red magnitude on the date having the majority of observations.
[b] Number of nights used to determine the light curve.
[c] Peak-to-peak range of the light curve.
[d] The light-curve period if there is one maximum per period.
[e] The light-curve period if there are two maxima per period.
[f] See Jewitt & Sheppard 2002 for details.

$B-V = 0.92 \pm 0.04$, $V-R = 0.63 \pm 0.03$, and $R-I = 0.56 \pm 0.03$ (Tables 5 and 6) show that 2000 GN$_{171}$ is red but unremarkably so as a KBO (Jewitt & Luu 2001).

3.3. (33128) 1998 BU$_{48}$

The KBO 1998 BU$_{48}$ showed substantial variability (>0.4 mag with period greater than 4.0 hr) in R-band observations from two nights in 2001 February and April. However, a convincing light curve could not be found from just these two nights separated by 2 months. Additional observations were obtained in the period 2001 November 14–19. One minimum and one maximum in brightness within a single night were observed and put the full single-peaked light curve between about 4 and 6 hr. Through PDM analysis, 1998 BU$_{48}$ was found to have a peak-to-peak variation of

$\Delta m = 0.68 \pm 0.04$ mag with possible single-peaked periods near 4.1, 4.9, and 6.3 hr, which are 24 hr aliases of each other (Fig. 7). By examining the phased data using these three possible periods, we find that the single-peaked periods of 4.9 ± 0.1 and 6.3 ± 0.1 hr are both plausible (Fig. 8). The colors, $B-V = 0.77 \pm 0.05$, $V-R = 0.68 \pm 0.04$, and $R-I = 0.50 \pm 0.04$ (Table 5), show no sign of variation throughout the light curve, within the measurement uncertainties (Table 7 and Fig. 8).

3.4. (40314) 1999 KR$_{16}$

This object was observed on four different observing runs during the course of 2000 and 2001. The data from 2001 are

TABLE 5
Colors of Observed Kuiper Belt Objects

Object		$B-V$	$V-R$	$R-I$
(38628)	2000 EB$_{173}$[a]	0.93 ± 0.04	0.65 ± 0.03	0.59 ± 0.03
(20000) Varuna	2000 WR$_{106}$[b]	0.85 ± 0.01	0.64 ± 0.01	0.62 ± 0.01
(26375)	1999 DE$_9$[a]	0.94 ± 0.03	0.57 ± 0.03	0.56 ± 0.03
(26181)	1996 GQ$_{21}$........	...	0.69 ± 0.03	...
	2000 GN$_{171}$	0.92 ± 0.04	0.63 ± 0.03	0.56 ± 0.03
(19521) Chaos	1998 WH$_{24}$[c]	0.94 ± 0.03	0.62 ± 0.03	...
(33340)	1998 VG$_{44}$[d]	0.93 ± 0.05	0.61 ± 0.04	0.77 ± 0.04
	2001 FZ$_{173}$	...	...	...
(33128)	1998 BU$_{48}$	0.77 ± 0.05	0.68 ± 0.04	0.50 ± 0.04
(40314)	1999 KR$_{16}$........	0.99 ± 0.05	0.75 ± 0.04	0.70 ± 0.05
	1997 CS$_{29}$[a]........	1.16 ± 0.06	0.61 ± 0.05	0.66 ± 0.05
	2001 CZ$_{31}$........	0.60 ± 0.15	0.5 ± 0.1	0.3 ± 0.1
	1998 HK$_{151}$[d].....	...	0.45 ± 0.04	0.42 ± 0.04

[a] From Jewitt & Luu 2001.
[b] See Jewitt & Sheppard 2002.
[c] From Tegler & Romanishin 2000.
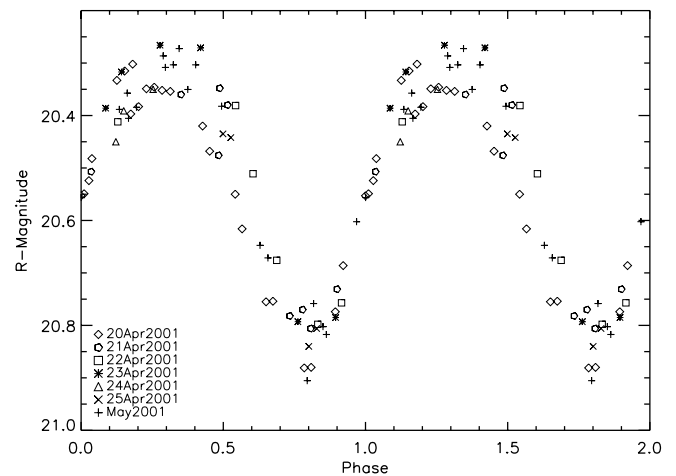[d] From Boehnhardt et al. 2001.

Fig. 2.—Phased R-band data from the UT 2001 April 20–25 and May 11–13 observations of 2000 GN$_{171}$. The period has been phased to 4.17 hr, which is the best-fit single-peaked period. The May data have been corrected for geometry and phase-angle differences relative to the April data (see Table 1). The points are much more scattered here than for the better fit double-peaked period (Fig. 3).
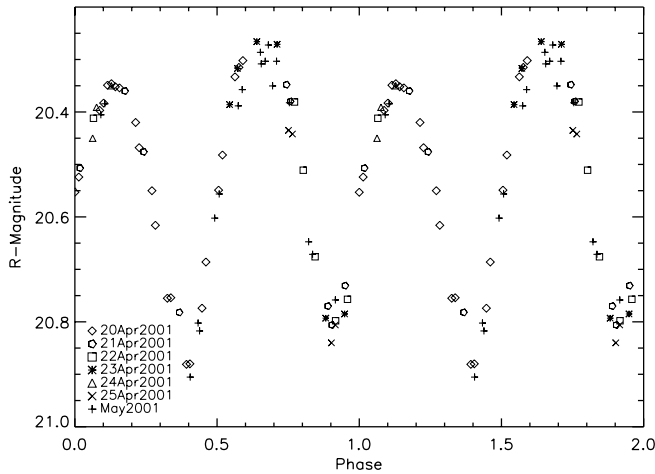
FIG. 3.—Same as Fig. 2, but the period has been phased to 8.329 hr, which is the best-fit double-peaked period.

more numerous and of better quality than the data from 2000. We observed one brightness minimum and one maximum within a single night of data and from this estimated that the full single-peaked light curve should be near 6 hr. In a PDM plot constructed using only the inferior data from 2000, we found single-peaked minima at 4.66 and 5.82 hr. Phased light curves at these periods are acceptable for the year 2000 data, but the 4.66 hr period is inconsistent with the data from 2001. In the PDM plot using the R-band data from 2001 February, April, and May, the best-fit single-peaked period is shown to be around 5.9 hr with associated flanking peaks from 24 hr and 15 and 60 day sampling aliases (Fig. 9). Closer examination of the PDM fit near 5.9 hr shows the 15 and 60 day aliasing much better and gives two best-fit periods, one at 5.840 hr and the other at 5.929 hr (Fig. 10). We phased the 2001 data to both single peaks and found neither to be significantly better than the other. The true single-peaked period for 1999 KR$_{16}$ is at one of these two values. The data phased to the 5.840 hr single-peaked
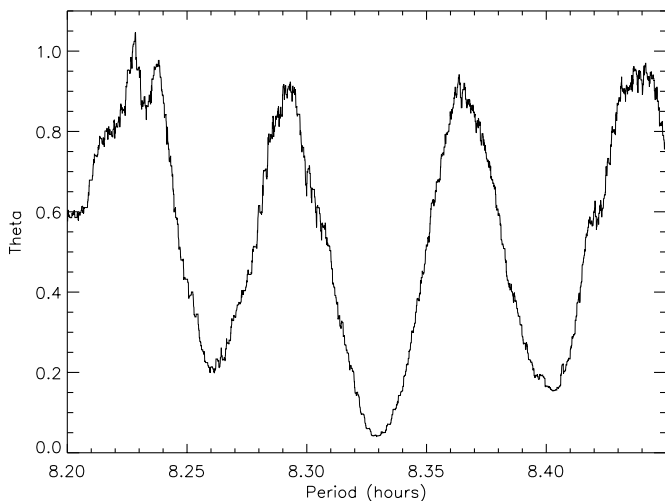
FIG. 4.—Closer view of the PDM plot for 2000 GN$_{171}$ around the doubled-peaked period near 8.33 hr. The best fit at 8.329 hr is flanked by aliases from the ~15 day separation of the two data sets obtained for this object.

period are shown in Figure 11. Neither of the possible double-peaked periods of 11.680 and 11.858 hr shows differences between the peaks. The peak-to-peak amplitude of 1999 KR$_{16}$ is 0.18 ± 0.04 in the 2001 data, consistent with that found in the 2000 data. Colors of 1999 KR$_{16}$, $B-V = 0.99 \pm 0.05$, $V-R = 0.75 \pm 0.04$, and $R-I = 0.70 \pm 0.04$, are on the red end of the KBO distribution (Table 5). The colors show no signs of variation through the rotation of the object to the accuracy of our measurements (Table 8 and Fig. 11).

3.5. Null Light Curves

Nine of the TNOs [2001 FZ$_{173}$, 2001 CZ$_{31}$, (38628) 2000 EB$_{173}$, (26375) 1999 DE$_9$, 1998 HK$_{151}$, (33340) 1998 VG$_{44}$, (19521) Chaos 1998 WH$_{24}$, 1997 CS$_{29}$, and (26181) 1996 GQ$_{21}$] show no measurable photometric variations. Practically, this means that their light curves have range ≤0.15 mag, period ≥24 hr, or both (Fig. 12 and Table 4). A few objects show hints of variability that might, with better data, emerge as rotationally modulated light curves. Inspection of the 2001 CZ$_{31}$ data hints at a single-peaked light curve of period ~3 hr and amplitude ~0.15 mag, but since the photometry has large error bars, we cannot be sure of this result. The TNO 1999 DE$_9$ may have a long-period light curve of about 0.1 mag range, since the brightness on 2001 April 24 slowly increases toward the end of the night and the February data appear to have base magnitudes different by about 0.1 mag. The data from 2000 on 1999 DE$_9$ show the object to have a flat light curve. The object (33340) 1998 VG$_{44}$ may also have a long-period light curve, since its base magnitudes on 1999 November 11 and 12 are different by about 0.05 mag. The bright TNO (19521) 1998 WH$_{24}$ may have a possible light curve of about 4 hours single-peaked period and peak-to-peak range of 0.07 mag. Confirmation of these subtle light curves will require more accurate data, probably from larger telescopes than that employed here.

4. INTERPRETATION

The KBOs should be in principal-axis rotation, since the expected damping time of any other wobbles is much less than the age of the solar system (Burns & Safronov 1973; Harris 1994). Orbital periods of KBOs are long (>200 yr), and thus the pole orientation to our line of sight should not change significantly between epochs. The apparent magnitude of a KBO depends on its physical characteristics and geometric circumstances and can be represented as

$$m_R = m_\odot - 2.5 \log[p_R r^2 \phi(\alpha)/(2.25 \times 10^{16} R^2 \Delta^2)] , \quad (1)$$

in which r (km) is the radius of the KBO, R (AU) is the heliocentric distance, Δ (AU) is the geocentric distance, $m_\odot$ is the apparent red magnitude of the Sun (−27.1), m_R is the apparent red magnitude, p_R is the red geometric albedo, and $\phi(\alpha)$ is the phase function, in which the phase angle $\alpha = 0°$ at opposition and $\phi(0) = 1$. The apparent brightness of an inert body viewed in reflected light may vary because of (a) changes in the observing geometry, including the effects of phase darkening as in equation (1), and (b) rotational modulation of the scattered light. These different effects are discussed below.
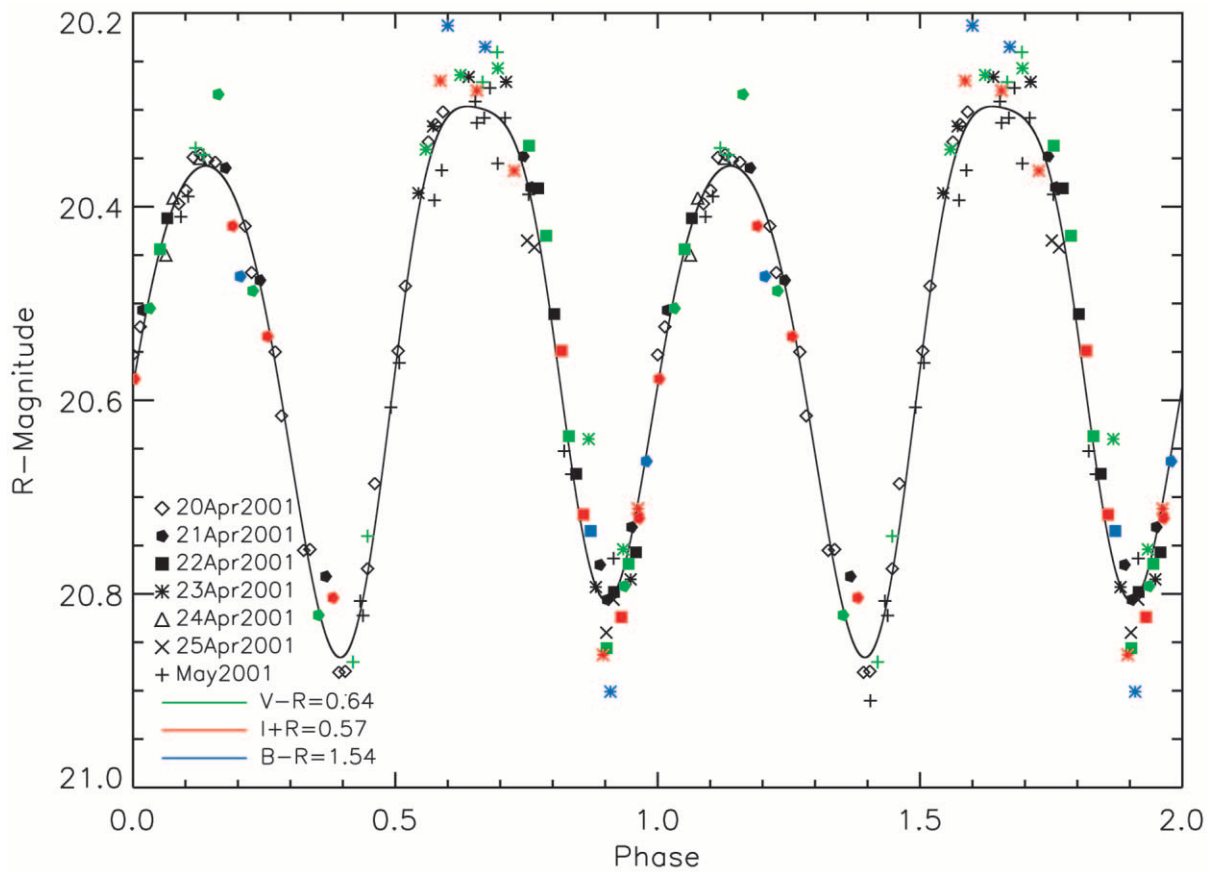
FIG. 5.—Same as Fig. 3, but for the *BVRI* data. The *BVI* data have been shifted by the amount indicated on the graph in order to correspond to the *R* data. No color variation is seen within our uncertainties. A Fourier fit shows the two pronounced maxima and minima.

4.1. *Nonuniform Surface Markings*

Surface albedo markings or topographical shadowing can potentially influence the light curves. Judging by other planetary bodies, the resulting light variations are typically smaller than those caused by elongated shape, with fluctuations due to albedo being mostly less than about 10%–20% (Degewij, Tedesco, & Zellner 1979). A color variation at the maximum and minimum of a light curve may be seen if albedo is the primary cause for the light curve, since materials with markedly different albedos often also have markedly different colors. For example, many pure ices and frosts have a very high albedo and are neutral to bluish in color. A light curve caused by an ice or frost patch should show a
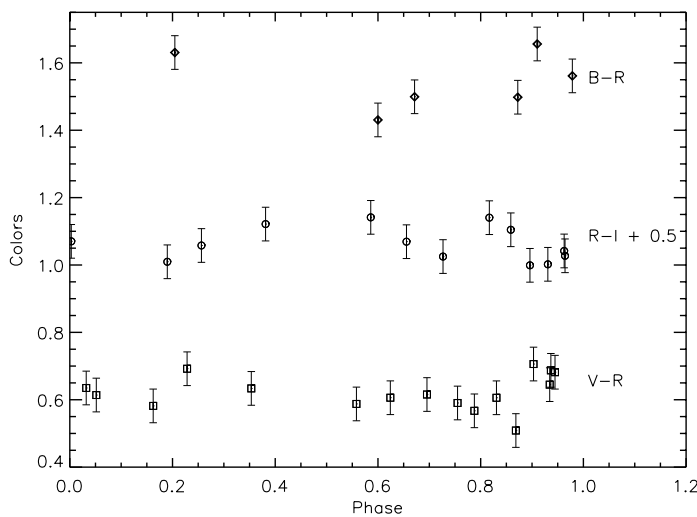
FIG. 6.—Colors of 2000 GN$_{171}$ plotted against rotational phase for 8.329 hr.
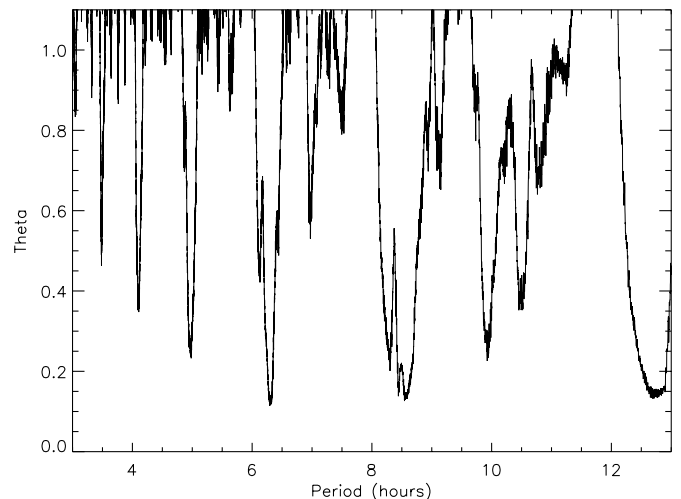
FIG. 7.—PDM plot for (33128) 1998 BU$_{48}$ from the 2001 November data. Best fits from this plot are the 4.9 and 6.3 hr single-peaked fits and the 9.8 and 12.6 hr double-peaked fits.

PHOTOMETRY OF KUIPER BELT OBJECTS

TABLE 6
COLOR MEASUREMENTS OF 2000 GN$_{171}$

Image	UT Date	JD$_c$[a]	Phase[b]	R[c]	B−R	V−R	R−I
2049	2001 Apr 21.3523	2,452,020.8523	0.937	20.745	...	0.687	...
2055	2001 Apr 21.3853	2,452,020.8853	0.032	20.510	...	0.635	...
2067	2001 Apr 21.4306	2,452,020.9306	0.162	20.342	...	0.582	...
2071	2001 Apr 21.4535	2,452,020.9535	0.228	20.435	...	0.692	...
2080	2001 Apr 21.4969	2,452,020.9969	0.353	20.828	...	0.634	...
2051	2001 Apr 21.3619	2,452,020.8619	0.964	20.679	...	...	0.527
2053	2001 Apr 21.3753	2,452,020.8752	0.003	20.578	...	...	0.570
2069	2001 Apr 21.4401	2,452,020.9401	0.190	20.360	...	...	0.510
2073	2001 Apr 21.4632	2,452,020.9632	0.256	20.522	...	...	0.558
2082	2001 Apr 21.5066	2,452,021.0066	0.381	20.856	...	...	0.621
2052	2001 Apr 21.3668	2,452,020.8668	0.979	20.642	1.561	...	...
2070	2001 Apr 21.4452	2,452,020.9452	0.205	20.381	1.631	...	...
3052	2001 Apr 22.3304	2,452,021.8303	0.755	20.387	...	0.590	...
3054	2001 Apr 22.3417	2,452,021.8417	0.788	20.503	...	0.567	...
3057	2001 Apr 22.3566	2,452,021.8566	0.831	20.671	...	0.606	...
3061	2001 Apr 22.3817	2,452,021.8817	0.903	20.790	...	0.706	...
3064	2001 Apr 22.3962	2,452,021.8962	0.945	20.727	...	0.682	...
3074	2001 Apr 22.4333	2,452,021.9333	0.052	20.470	...	0.614	...
3056	2001 Apr 22.3518	2,452,021.8518	0.817	20.620	...	...	0.640
3059	2001 Apr 22.3663	2,452,021.8663	0.859	20.753	...	...	0.605
3063	2001 Apr 22.3914	2,452,021.8914	0.931	20.756	...	...	0.502
3060	2001 Apr 22.3711	2,452,021.8711	0.872	20.777	1.498	...	...
4040	2001 Apr 23.3032	2,452,022.8031	0.558	20.393	...	0.588	...
4044	2001 Apr 23.3261	2,452,022.8261	0.624	20.298	...	0.606	...
4048	2001 Apr 23.3508	2,452,022.8508	0.695	20.281	...	0.616	...
4064	2001 Apr 23.4109	2,452,022.9109	0.869	20.771	...	0.509	...
4068	2001 Apr 23.4338	2,452,022.9338	0.934	20.749	...	0.645	...
4042	2001 Apr 23.3128	2,452,022.8128	0.586	20.341	...	...	0.641
4046	2001 Apr 23.3370	2,452,022.8370	0.656	20.279	...	...	0.569
4050	2001 Apr 23.3617	2,452,022.8616	0.727	20.318	...	...	0.525
4066	2001 Apr 23.4204	2,452,022.9204	0.896	20.792	...	...	0.499
4070	2001 Apr 23.4435	2,452,022.9435	0.963	20.684	...	...	0.542
4043	2001 Apr 23.3177	2,452,022.8177	0.600	20.322	1.431	...	...
4047	2001 Apr 23.3424	2,452,022.8424	0.671	20.276	1.499	...	...
4067	2001 Apr 23.4253	2,452,022.9253	0.910	20.785	1.656	...	...
3029[d]	2001 May 13.2793	2,452,042.7793	0.119	20.366	...	0.614	...
3030[d]	2001 May 13.2847	2,452,042.7847	0.135	20.352	...	0.635	...
3053[d]	2001 May 13.3834	2,452,042.8834	0.419	20.823	...	0.688	...
3055[d]	2001 May 13.3931	2,452,042.8931	0.447	20.753	...	0.627	...
3068[d]	2001 May 13.4691	2,452,042.9691	0.666	20.276	...	0.635	...
3070[d]	2001 May 13.4788	2,452,042.9788	0.694	20.281	...	0.600	...
Mean.......					1.55 ± 0.03	0.63 ± 0.03	0.56 ± 0.03

[a] Julian day at start of exposure.

[b] Phase of 2000 GN$_{171}$ corresponding to color measurement. Phases of 0.2 and 0.7 correspond to maximum brightness (∼20.3), and 0.4 and 0.9 correspond to minimum brightness (∼20.9).

[c] R magnitude interpolated to the time of the corresponding BVI data.

[d] R and V magnitudes are corrected for phase and distance difference from April data.

bluish color when at maximum brightness. Some of the most extreme albedo contrasts are found on Pluto and the Saturnian satellite Iapetus (Table 9). The latter is in synchronous rotation around Saturn, with its leading hemisphere covered in a very low albedo material thought to be deposited from elsewhere in the Saturnian system. Iapetus shows clear rotational color variations [$\Delta(B-V) \sim 0.1$ mag] that are correlated with the rotational albedo variations. On the other hand, Pluto has large albedo differences across its surface, but the hemispherically averaged color variations are only of order 0.01 mag. We feel that neither Iapetus nor Pluto constitutes a particularly good model for the KBOs. The large albedo contrast on Iapetus is a special consequence of its synchronous rotation and the impact of material trapped in orbit about Saturn. This process is with-

out analog in the Kuiper belt. Pluto is also not representative of the other KBOs. It is so large that it can sustain an atmosphere, which may contribute to amplifying its light-curve amplitude by allowing surface frosts to condense on brighter (cooler) spots. Thus, brighter spots grow brighter while darker (hotter) spots grow darker through the sublimation of ices. This positive feedback mechanism requires an atmosphere and is unlikely to be relevant on the smaller KBOs studied here.

4.2. Aspherical Shape

The critical rotation period ($T_{\rm crit}$) at which centripetal acceleration equals gravitational acceleration toward the
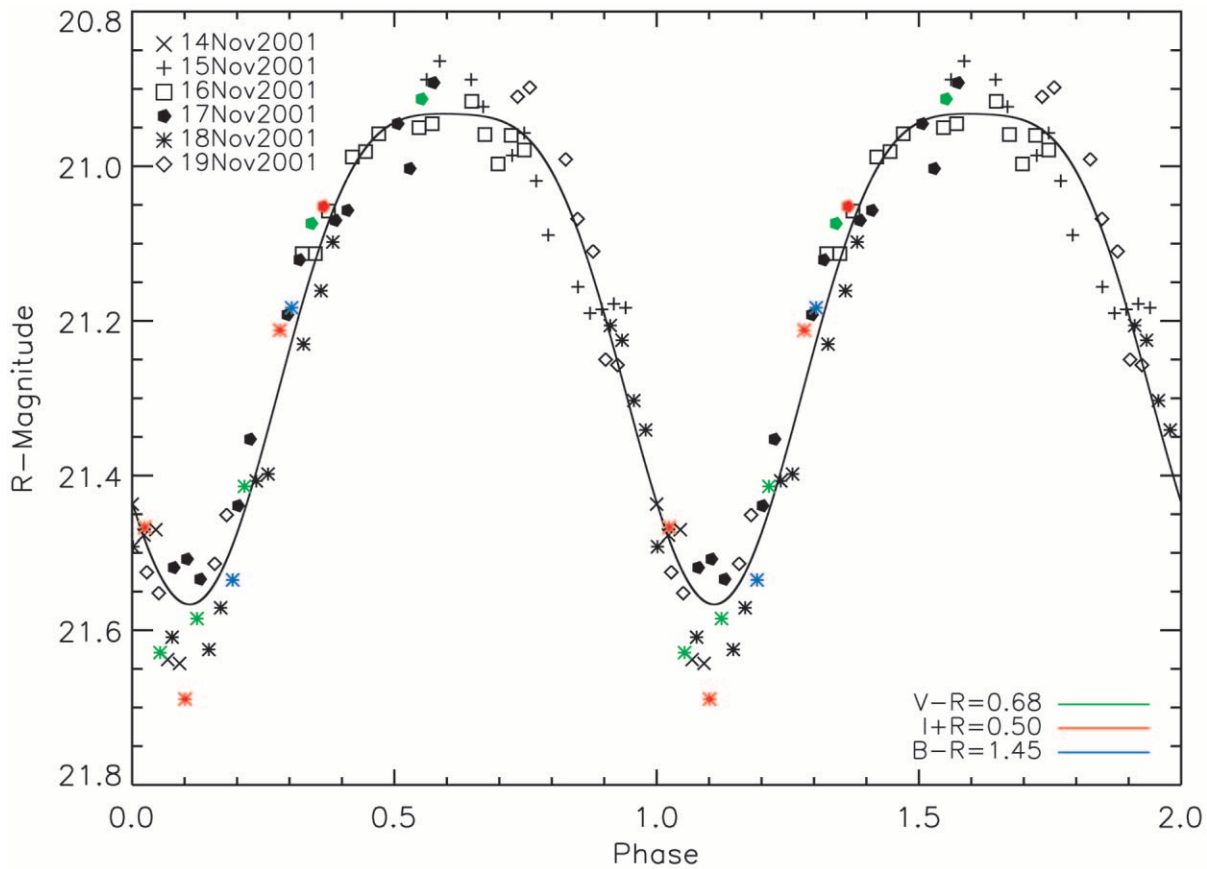
FIG. 8.—*BVRI* phased data from the UT 2001 November 14–19 observations of (33128) 1998 BU$_{48}$. The period has been phased to 6.29 hr, which is one of the best-fit single-peaked periods for (33128) 1998 BU$_{48}$, the other being around 4.9 hr.

center of a rotating spherical object is

$$T_{\mathrm{crit}} = \left(\frac{3\pi}{G\rho} \right)^{1/2}, \qquad (2)$$

where G is the gravitational constant and ρ is the density of the object. With $\rho = 10^3 \ \mathrm{kg \ m^{-3}}$, the critical period is about 3.3 hr. Even at longer periods, real bodies will suffer centri-

petal deformation into aspherical shapes. For a given density and specific angular momentum (H), the nature of the deformation depends on the strength of the object. In the limiting case of a strengthless (fluid) body, the equilibrium shapes have been well studied (Chandrasekhar 1987). For $H \leq 0.304$ [in units of $(GM^3 a')^{1/2}$, where M (kg) is the mass of the object and a' (m) is the radius of an equal-volume sphere], the equilibrium shapes are the oblate "Maclaurin"

TABLE 7
COLOR MEASUREMENTS OF (33128) 1998 BU$_{48}$

Image	UT Date	JD$_c$[a]	Phase[b]	R[c]	B−R	V−R	R−I
4098	2001 Nov 17.5907	2,452,231.0907	0.3418	21.138	...	0.613	...
4107	2001 Nov 17.6458	2,452,231.1458	0.5519	20.934	...	0.656	...
4099	2001 Nov 17.5968	2,452,231.0967	0.3647	21.091	...	...	0.542
5088	2001 Nov 18.5635	2,452,231.9666	0.1916	21.490	1.497	...	...
5091	2001 Nov 18.5819	2,452,231.9850	0.3042	21.227	1.408	...	...
5095	2001 Nov 18.6056	2,452,232.0087	0.0533	21.529	...	0.777	...
5087	2001 Nov 18.5558	2,452,231.9589	0.1237	21.564	...	0.698	...
5090	2001 Nov 18.5760	2,452,231.9791	0.2141	21.446	...	0.645	...
5098	2001 Nov 18.6233	2,452,232.0264	0.0242	21.483	...	...	0.519
5094	2001 Nov 18.5997	2,452,232.0028	0.1011	21.566	...	...	0.380
5099	2001 Nov 18.6292	2,452,232.0323	0.2817	21.283	...	...	0.574
Mean.......					1.45 ± 0.05	0.68 ± 0.04	0.50 ± 0.04

[a] Julian day at start of exposure.
[b] Phase of (33128) 1998 BU$_{48}$ corresponding to color measurement of the single-peaked 6.29 hr light curve. The phase of 0.6 corresponds to maximum brightness (∼20.9), and 0.1 corresponds to minimum brightness (∼21.6).
[c] R magnitude interpolated to the time of the corresponding *BVI* data.
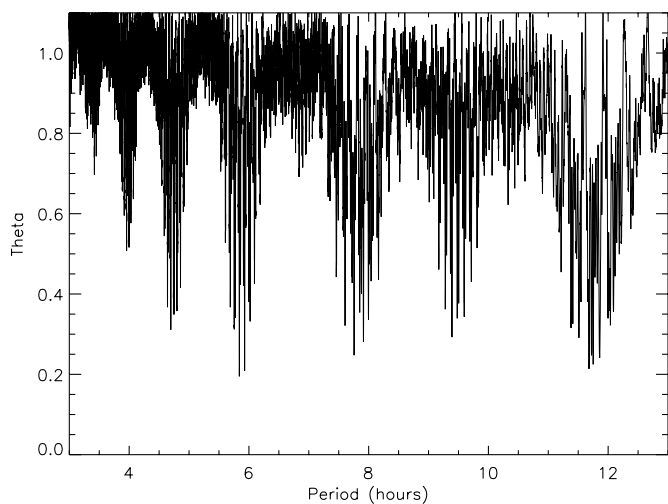
FIG. 9.—PDM plot for (40314) 1999 KR$_{16}$ using all the R-band data from 2001 February, April, and May. Best fits from this plot are near the 5.9 hr single-peak period and the 11.8 hr double-peaked period. Both are flanked by aliases of the 24 hr and ∼15 and ∼60 day sampling periodicities.

spheroids. Oblate spheroids in rotation about their minor axis exhibit no rotational modulation of the cross section and therefore are not candidate shapes for explaining the light curves of the KBOs. However, for $0.304 \leq H \leq 0.390$ the equilibrium figures are triaxial "Jacobi" ellipsoids, which generate light curves of substantial amplitude when viewed equatorially. Strengthless objects with $H > 0.390$ are rotationally unstable to fission.

The KBOs, being composed of solid matter, clearly cannot be strengthless. However, it is likely that the interior structures of these bodies have been repeatedly fractured by impact, and that their mechanical response to applied rotational stress is approximately fluid-like. Such "rubble pile" structure has long been suspected in the main asteroid belt (Farinella et al. 1981) and has been specifically proposed to explain the short period and large amplitude of (20000) Varuna (Jewitt & Sheppard 2002). The rotational deforma-

tion of a rubble pile is uniquely related to its bulk density and specific angular momentum. Therefore, given that the shape and specific angular momentum can be estimated from the amplitude and period of the light curve, it is possible to use photometric data to estimate the density.
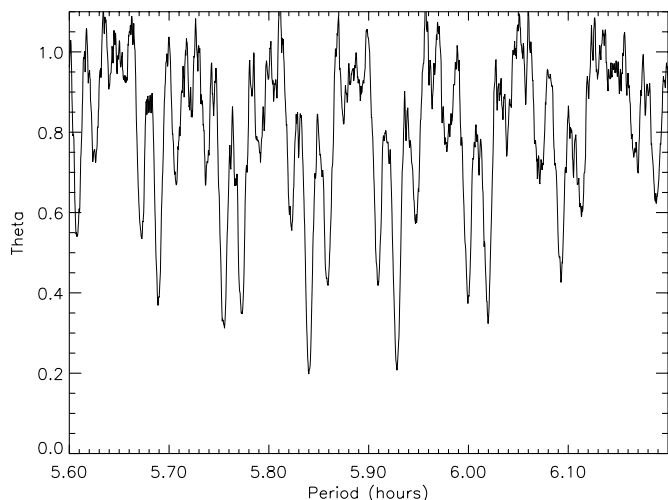
Elongated objects exhibit rotational photometric variations caused by changes in the projected cross section. The rotation period of an elongated object should be twice the single-peaked light-curve variation because of its projection of both long axes (two maxima) and short axes (two minima) during one full rotation. From the ratio of maximum to minimum brightness, we can determine the projection of the body shape into the plane of the sky. The rotational brightness range of a triaxial object with semiaxes $a \geq b \geq c$ in rotation about the c-axis is given by

$$\Delta m = 2.5 \log \left(\frac{a}{b} \right) - 1.25 \log \left(\frac{a^2 \cos^2 \theta + c^2 \sin^2 \theta}{b^2 \cos^2 \theta + c^2 \sin^2 \theta} \right) \quad (3)$$

(Binzel et al. 1989), where Δm is expressed in magnitudes and θ is the angle at which the rotation (c) axis is inclined to the line of sight (an object with $\theta = 90°$ is viewed equatorially).

It is to be expected that, through collisions, fragments would have random pole-vector orientations. For example, the collisionally highly evolved asteroid belt shows a complete randomization of pole-vector orientations, θ. Only the largest asteroids may show a preference for rotation vectors aligned perpendicular to the ecliptic ($\theta = 90°$), though this is debatable (Binzel et al. 1989; Drummond et al. 1991; De Angelis 1995). In the absence of any pole orientation data for the KBOs, we will assume they have a random distribution of spin vectors. Given a random distribution, the probability of viewing an object within the angle range θ to $\theta + d\theta$ is proportional to $\sin \theta \, d\theta$. In such a distribution, the average viewing angle is $\theta = 60°$. Therefore, on average, the sky-plane ratio of the axes of an elongated body is smaller than the actual ratio by a factor $\sin 60° \approx 0.87$.

In addition to rotational deformation, it is possible that some asteroids and KBOs consist of contact binaries (Jewitt & Sheppard 2002). For a contact binary consisting of equal spheres, the axis ratio of 2:1 corresponds to a peak-to-peak light-curve range $\Delta m = 0.75$ mag, as seen from the rotational equator. For such an object at the average viewing angle $\theta = 60°$, we expect $\Delta m = 0.45$ mag.

Collisionally produced fragments on average have axis ratios $2 : \sqrt{2} : 1$ (Fujiwara, Kamimoto, & Tsukamoto 1978; Capaccioni et al. 1984). When viewed equatorially, such fragments will have $\Delta m = 0.38$ mag. At the mean viewing angle $\theta = 60°$, we obtain $\Delta m = 0.20$ mag.

4.3. Light-Curve Model Results

The KBOs in our sample are very large ($D > 250$ km, assuming a low albedo) and should, in the absence of rotational deformation, be spherical in shape from gravitational self-compression. The large amplitudes and fast rotations of (20000) Varuna, 2000 GN$_{171}$, and (33128) 1998 BU$_{48}$ suggest that the light curves are caused by elongation and not surface albedo features. In support of this is the finding that (33128) 1998 BU$_{48}$ and (20000) Varuna have no color variations throughout their light curves and 2000 GN$_{171}$ has only a slight, if any, variation in color. Independently, 2000 GN$_{171}$ shows two distinct light-curve maxima and minima,

FIG. 10.—Closer view of the PDM plot for (40314) 1999 KR$_{16}$ around the best-fit single-peaked periods near 5.9 hr.
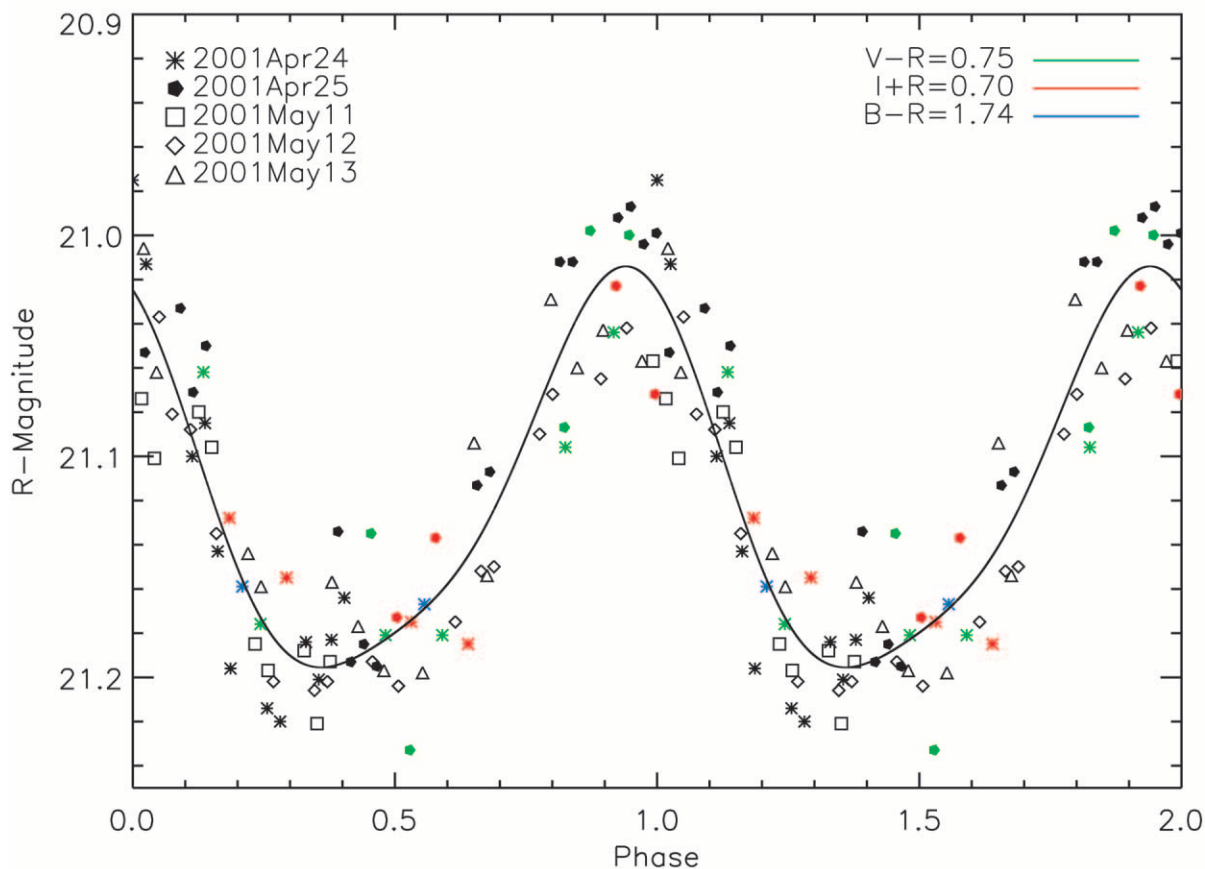
Fig. 11.—Phased *BVRI* data from the UT 2001 April 24–25 and May 11–13 observations of (40341) 1999 KR$_{16}$. The period has been phased to 5.840 hr, which is one of the best-fit single-peaked periods for (40341) 1999 KR$_{16}$, the other being at 5.929 hr.

TABLE 8
Color Measurements of (40341) 1999 KR$_{16}$

Image	UT Date	JD$_c$[a]	Phase[b]	R[c]	$B-R$	$V-R$	$R-I$
2031	2001 May 12.2634	2,452,041.7634	0.135	21.107	...	0.705	...
2035	2001 May 12.2899	2,452,041.7899	0.244	21.173	...	0.753	...
2051	2001 May 12.3479	2,452,041.8479	0.482	21.183	...	0.748	...
2055	2001 May 12.3743	2,452,041.8743	0.590	21.161	...	0.770	...
2069	2001 May 12.4314	2,452,041.9314	0.825	21.048	...	0.798	...
2073	2001 May 12.4538	2,452,041.9538	0.917	21.016	...	0.778	...
2033	2001 May 12.2754	2,452,041.7754	0.184	21.141	...	...	0.713
2037	2001 May 12.3020	2,452,041.8019	0.293	21.189	...	...	0.734
2053	2001 May 12.3599	2,452,041.8599	0.531	21.174	...	...	0.699
2057	2001 May 12.3862	2,452,041.8862	0.640	21.145	...	...	0.660
2034	2001 May 12.2815	2,452,041.7814	0.209	21.156	1.743	...	...
2054	2001 May 12.3659	2,452,041.8659	0.556	21.169	1.738	...	...
3035	2001 May 13.3145	2,452,042.8144	0.454	21.187	...	0.698	...
3038	2001 May 13.3325	2,452,042.8325	0.528	21.175	...	0.808	...
3057	2001 May 13.4042	2,452,042.9042	0.823	21.050	...	0.787	...
3059	2001 May 13.4162	2,452,042.9161	0.872	21.027	...	0.721	...
3062	2001 May 13.4342	2,452,042.9342	0.947	21.014	...	0.736	...
3037	2001 May 13.3265	2,452,042.8265	0.504	21.179	...	...	0.706
3040	2001 May 13.3444	2,452,042.8444	0.577	21.164	...	...	0.727
3061	2001 May 13.4282	2,452,042.9282	0.922	21.015	...	...	0.692
3064	2001 May 13.4463	2,452,042.9463	0.996	21.023	...	...	0.652
Mean.......					1.74 ± 0.04	0.75 ± 0.03	0.70 ± 0.03

[a] Julian day at start of exposure.

[b] Phase of (40341) 1999 KR$_{16}$ corresponding to color measurement of the single-peaked 5.84 hr light curve. The phase of 0.9 corresponds to maximum brightness (~21.0), and 0.4 corresponds to minimum brightness (~21.2).

[c] *R* magnitude interpolated to the time of the corresponding *BVI* data. *R* magnitudes are corrected for phase and distance difference from April data so they can be compared with the plots directly.
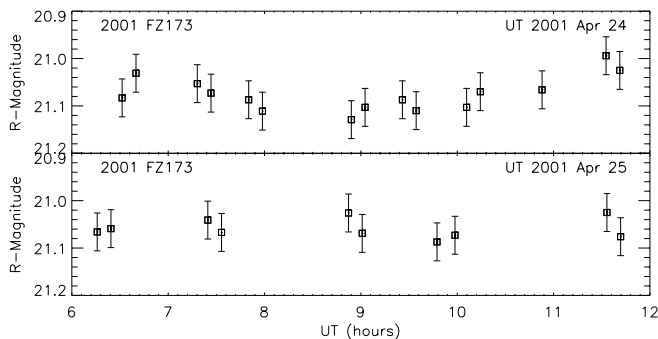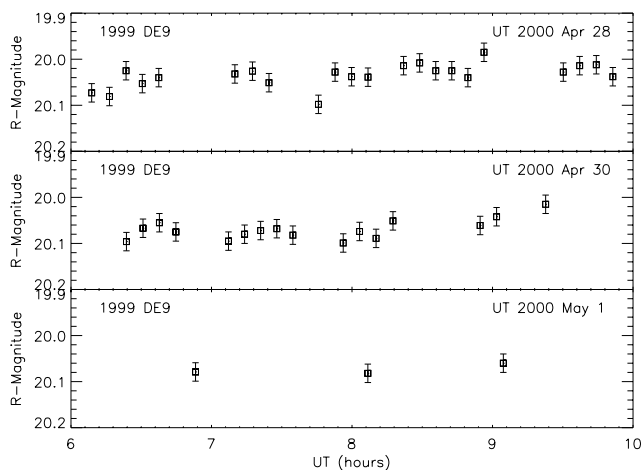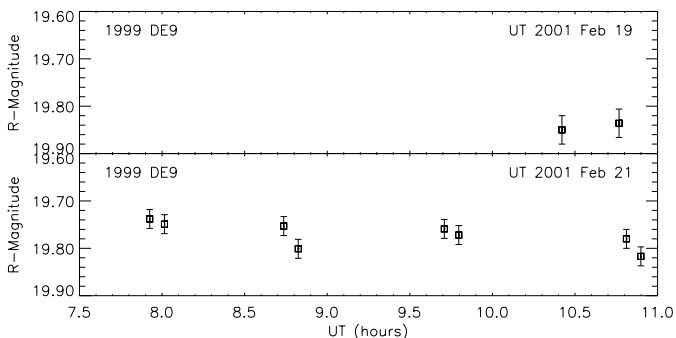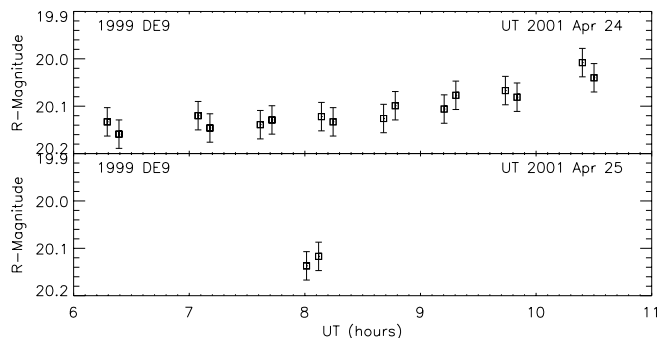
Fig. 12a
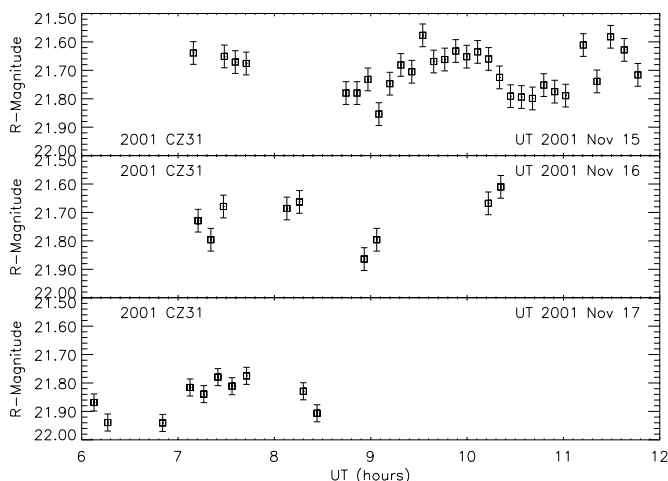
Fig. 12b
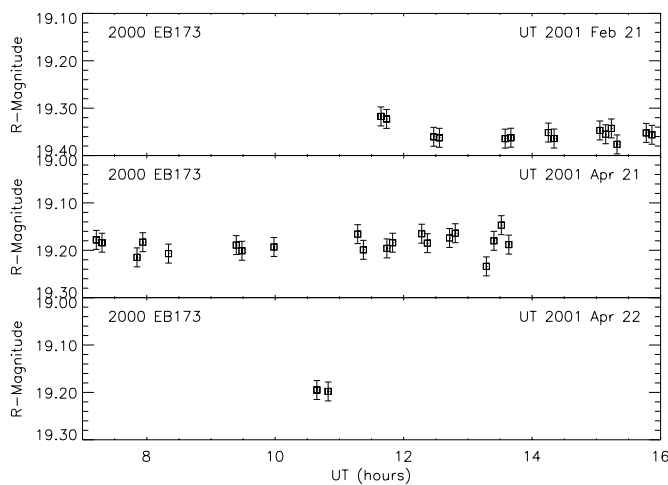
Fig. 12c

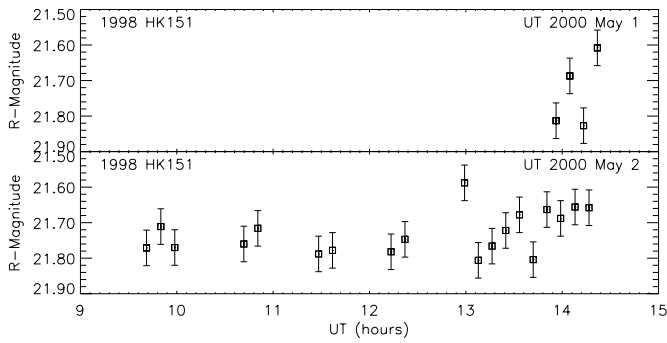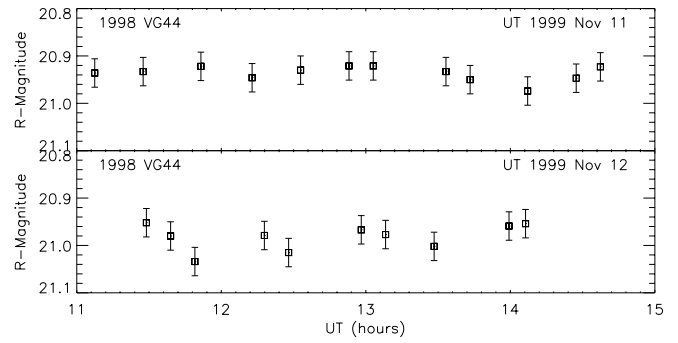Fig. 12d

Fig. 12e

Fig. 12f

Fig. 12.—Null light curves of KBOs found to have no significant variation: (a) 2001 FZ$_{173}$, (b) 2001 CZ$_{31}$, (c) (38628) 2000 EB$_{173}$, (d–f) (26375) 1999 DE$_9$, (g) 1998 HK$_{151}$, (h) (33340) 1998 VG$_{44}$, (i) (19521) Chaos 1998 WH$_{24}$, (j) 1997 CS$_{29}$, (k–l) (26181) 1996 GQ$_{21}$.

which is a strong reason to believe the object is elongated. The other light curve we found was for (40314) 1999 KR$_{16}$. Since its amplitude is much smaller and its period longer, the light curve of (40314) 1999 KR$_{16}$ may be more dominated by nonuniform-albedo features on its surface, though we found no measurable color variation over the rotation.

Table 10 lists the parameters of albedo, Jacobi ellipsoid, and binary models that fit the axis ratios estimated from the light-curve data (Table 4). For each object and model, we list the minimum bulk density ρ required to maintain a stable configuration, as described in Jewitt & Sheppard (2002). We briefly describe the procedure below for 2000 GN$_{171}$. Results for the rest of the objects in our sample with significant light variation [(20000) Varuna, (33128) 1998 BU$_{48}$, and (40314) 1999 KR$_{16}$] can be seen in Table 10, using the data from Table 4.

Fig. 12g

Fig. 12h
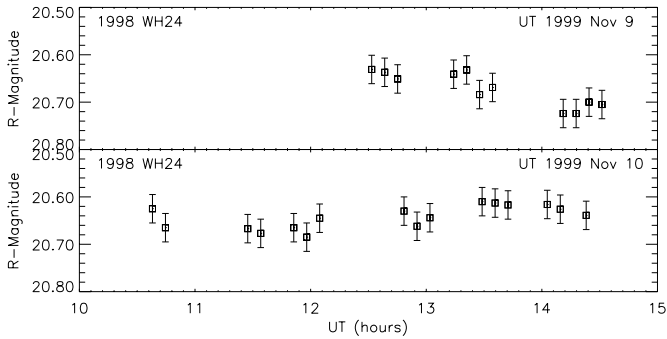
Fig. 12i
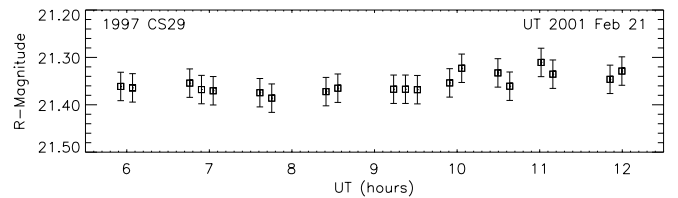
Fig. 12j
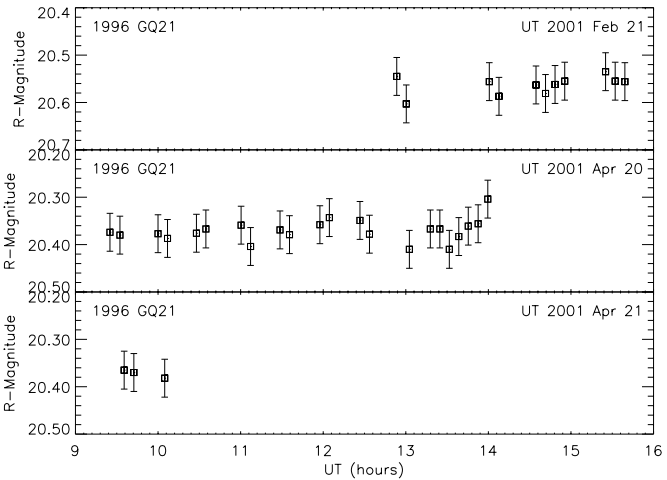
Fig. 12k
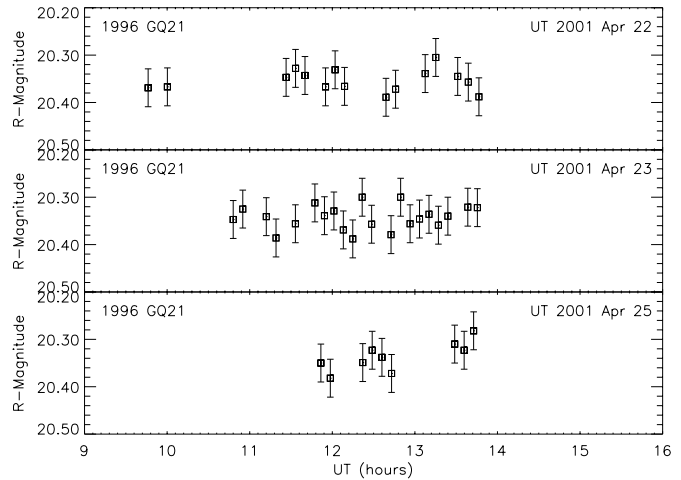
Fig. 12l

We use equation (3) to estimate the axis ratio a/b. If we assume that the rotation axis is perpendicular to our line of sight ($\theta = 90°$), we obtain

$$a/b = 10^{0.4 \Delta m_R} . \qquad (4)$$

Using $\Delta m_R = 0.61$ mag, we obtain from equation (4) $a/b = 1.75 : 1$ for 2000 GN_{171}. This is a lower limit to the intrinsic axis ratio because of the effects of projection into the plane of the sky. If 2000 GN_{171} is a Jacobi triaxial ellipsoid with $P = 8.329$ hr, then its $a : b : c$ axis ratio would be $1.75 : 1 : 0.735$ and the lower limit on the density would be $\rho = 635$ kg m^{-3} (Chandrasekhar 1987; see Jewitt & Sheppard 2002 for a KBO-context discussion of Jacobi ellipsoids). If 2000 GN_{171} were a contact binary, the ratio of the two radii, $a_1 : a_2$, would be $1.15 : 1$ with a lower limit to the

density of $\rho = 585$ kg m^{-3} (see Jewitt & Sheppard 2002 for a discussion of contact binaries in the KBO context). Finally, though it is unlikely, if 2000 GN_{171} is spherical and the light curve is due to a $1.75 : 1$ contrast in albedo, then the lower limit to the density of the KBO is $\rho = 157$ kg m^{-3} from equation (2) and using $P = 8.329$ hr.

5. DISCUSSION

In Table 9, we show objects in the solar system that have one axis of at least 200 km and show large-amplitude light curves. Interestingly, there is a group of asteroids that are large ($D = 200$–300 km) and which have substantial light-curve amplitudes. They also possess fast rotations. These objects are probably rotationally deformed "rubble piles," which may be similar to a Jacobi ellipsoid–type object

TABLE 9
LIST OF LARGE OBJECTS WITH LARGE-AMPLITUDE LIGHT CURVES

Name	Type	$a \times b \times c$ (km)	ρ (kg m^{-3})	Δ mag	Period (hr)	Comment
Pluto	Planet	2300	2061	0.33	6.4 days	Albedo
Iapetus	Satellite	1430	1025	2	79.3 days	Albedo
Hyperion	Satellite	$350 \times 240 \times 200$	$\sim$1250	0.5	Chaos	Fragment?
624 Hektor	Trojan	300×150	$\sim$2500	1.2	6.9	Contact binary?
Amalthea	Satellite	$270 \times 166 \times 150$	$\sim$3000	...	...	Fragment (?)/albedo
15 Eunomia	Asteroid	$\sim$270 $\times$ 160 $\times$ 115	1160	0.56	6.1	Jacobi?
87 Sylvia	Asteroid	$\sim$270 $\times$ 150 $\times$ 115	1640	0.62	5.2	Jacobi?
16 Psyche	Asteroid	$\sim$260 $\times$ 175 $\times$ 120	2340	0.42	4.2	Jacobi?
107 Camilla	Asteroid	$\sim$240 $\times$ 150 $\times$ 105	1850	0.52	4.8	Jacobi?
Janus.................	Satellite	$220 \times 190 \times 160$	656	...	...	Fragment?
45 Eugenia	Asteroid	$\sim$210 $\times$ 145 $\times$ 100	1270	0.41	5.7	Jacobi?

NOTE.—Listed are objects that have diameters over 200 km and light curves with peak-to-peak amplitudes above 0.40 mag. Pluto is the only exception, since its light curve is slightly less than 0.40 mag. The Jacobi-type main-belt asteroids had their axis ratios and densities calculated from their amplitudes and periods as described for the KBOs in the text. Data for the other objects were culled from the best measurements in the literature.

(Farinella et al. 1981). Such rubble-pile structures may form in the main asteroid belt because all objects have been affected by the high-velocity ($\sim$5 km s^{-1}) collisions that occur there (Farinella, Paolicchi, & Zappalà 1982). The effect of collisions is highly dependent on the object size. Objects with $D > 300$ km are large enough not to be completely turned into rubble piles or have their angular momentum greatly altered. Objects with diameters 200–300 km are large enough to be gravitationally bound, but impacts over the age of the solar system will transform them into rubble piles and may significantly change their angular momentum. Most asteroids with $D < 200$ km are thought to be fragments from catastrophic collisions and are not massive enough to be gravitationally spherical.

How does the collisional outcome scale with velocity and density differences in the asteroid belt versus the Kuiper belt? We assume the target body experiences catastrophic breakup when the projectile kinetic energy equals the gravitational binding energy of the target,

$$\frac{1}{2} M_p \Delta v^2 = \frac{3GM_t^2}{5r_t} , \qquad (5)$$

where Δv is the mean collision speed, M is mass, r is radius, and subscripts p and t refer to projectile and target, respectively. For collisions with a target of given radius, the ratio of the sizes of the projectiles needed to cause disruption in the main belt and in the Kuiper belt is

$$\frac{r_{p,\mathrm{KB}}}{r_{p,\mathrm{MB}}} = \left[\left(\frac{\rho_{t,\mathrm{MB}}}{\rho_{t,\mathrm{KB}}} \right) \left(\frac{\Delta v_{\mathrm{KB}}}{\Delta v_{\mathrm{MB}}} \right)^2 \right]^{-1/3} , \qquad (6)$$

where we have assumed that all KBOs have density ρ_{KB} and all main-belt asteroids have density ρ_{MB}. Here $r_{p,\mathrm{MB}}$ and $r_{p,\mathrm{KB}}$ are the radii of the projectile in the main belt and in the Kuiper belt that are needed to fracture the target in the respective belt, $\rho_{t,\mathrm{MB}}$ and $\rho_{t,\mathrm{KB}}$ are the densities of the target body in the main belt and Kuiper belt, respectively, and Δv_{MB} and Δv_{KB} are the respective collision velocities. If we put in nominal values of $\rho_{t,\mathrm{MB}} = 3000$ kg m^{-3}, $v_{\mathrm{MB}} = 5$ km s^{-1} and $\rho_{t,\mathrm{KB}} = 1000$ kg m^{-3}, $v_{\mathrm{KB}} = 1.5$ km s^{-1} for the main-belt asteroids and Kuiper belt, respectively, we find

$$r_{p,\mathrm{KB}} \approx 1.5 r_{p,\mathrm{MB}} . \qquad (7)$$

Thus, for targets of equal size a projectile has to be about 50% larger in the Kuiper belt than in the main belt to be able to cause catastrophic breakup of the target body. This difference is not large, and since the current collisional timescales for the asteroids and KBOs are similar (Davis & Farinella 1997; Durda & Stern 2000), other factors such as material strength and the number density of objects during early formation of each belt will be most important in determining collisional differences.

TABLE 10
SHAPE MODELS AND DENSITIES FOR KBOs WITH LIGHT CURVES

NAME	H (mag)	D[a] (km)	ALBEDO		JACOBI		BINARY	
			$a:b$	ρ	$a:b:c$	ρ	$a_1:a_2$	ρ
Varuna[b]	3.7	900	1:1	$\geq$1090	$\geq$1.5:1:0.7	$\geq$1050	$\geq$1.4:1	$\geq$996
2000 GN$_{171}$	5.8	400	1:1	$\geq$157	$\geq$1.75:1:0.74	$\geq$635	$\geq$1.15:1	$\geq$585
1998 BU$_{48}$	7.2	240	1:1	$\geq$109	$\geq$1.87:1:0.75	$\geq$456	$\geq$1.07:1	$\geq$435
1999 KR$_{16}$........	5.8	400	1:1	$\geq$77	$\geq$1.18:1:0.63	$\geq$280	$\geq$2.35:1	$\geq$210

[a] Diameter computed assuming that the albedo is 0.04.
[b] See Jewitt & Sheppard 2002.

The current Kuiper belt has been found to be erosive for KBOs with $D < 100$ km, while many of the larger objects are probably rubble piles (Davis & Farinella 1997). Laboratory and computer simulations show that self-gravitating targets are more easily fractured than dispersed (Asphaug et al. 1998). Once formed, rubble-pile structures can insulate the rest of the body from the energy of impact, further inhibiting disruption. Collision experiments by Ryan, Davis, & Giblin (1999) also show that porous ices dissipate energy efficiently. The outcome of impact into a rubble pile depends heavily on the angle of impact. We note that glancing low-velocity collisions substantially alter the spin of the target body and can create elongated objects and contact binaries (Leinhardt, Richardson, & Quinn 2000). These simulations all hint that rubble-pile structures are able to remain gravitationally bound after an impact but that their angular momentum may be altered in the process, which could produce elongated shapes.

To date, eight binary Kuiper belt objects have been reported. It seems that there may be a large fraction of binary KBOs. It also appears that about 32% of KBOs are highly elongated. Both the binaries and the highly elongated shapes indicate large specific angular momentum, most likely delivered by glancing collisions. The current rate of collisions is too small, however, for any substantial modifications of the spins or shapes of KBOs (Jewitt & Sheppard 2002). Instead, we prefer the hypothesis that the binaries and elongated shapes are products of an early, denser phase in the Kuiper belt, perhaps associated with its formation.

5.1. Other Light-Curve Observations

We now consider light-curve observations of KBOs published by others in order to make a larger sample. Unfortunately, few KBOs to date have been shown through independent observations to have repeatable light curves. Hainaut et al. (2000) reported that (19308) 1996 TO$_{66}$ has a light curve that varies in amplitude over the course of 1 year, and they interpreted this as a result of possible ongoing cometary activity. Object 1996 TO$_{66}$ may show a color difference throughout its rotation (Sekiguchi et al. 2002). In contrast, 1996 TO$_{66}$ was reported to have a flat light curve by Romanishin & Tegler (1999) during the same year in which Hainaut et al. detected variation. Our own observations show that 1996 TO$_{66}$ does have a significant light curve, basically confirming the variation originally observed by Hainaut et al. and contradicting the null detection by Romanishin & Tegler (Sheppard 2002). Conversely, an object reported to have a light curve by Romanishin & Tegler (1999), (15820) 1994 TB, was found by us to display no significant variation (Sheppard 2002). Because of these conflicts of unrepeatability, and since many of the Romanishin & Tegler targets were very sparsely sampled with raw data that remain unpublished, we use their work with caution in the following analysis.

Our combined sample of 22 KBOs comprises only well-observed objects with numerous observations that could constrain any significant photometric variation from this (Table 4) and other (Table 11) works. Among the objects newly observed in this survey (Table 4), the fraction with significant light-curve variation is $f(\Delta m_R \geq 0.15) = 4/13$ (31%) and $f(\Delta m_R \geq 0.40) = 3/13$ (23%). Including the objects reliably observed by others (Table 11) yields $f(\Delta m_R \geq 0.15) = 7/22$ (32%) and $f(\Delta m_R \geq 0.40) = 5/22$ (23%). Although we have evidence that some of their light curves are unrepeatable, we note that Romanishin & Tegler (1999) found a comparable $f(\Delta m_R \geq 0.10) = 3/11$ (27%). We consider these results all to point to a similar fraction $f(\Delta m_R \geq 0.15) \sim 32\%$ and $f(\Delta m_R \geq 0.40) \sim 23\%$.

The samples of objects with significant light curves and flat light curves were tested for correlations with orbital parameters and colors. No significant correlations were found. From the sample of 22 objects, two of the nine (22%) resonant objects, four of the eight (50%) classical objects, and one of the five (20%) scattered objects had measurable light curves ($\Delta m_R \geq 0.15$). Many of the objects shown in Table 11 are detailed elsewhere by us (Sheppard 2002) because they were objects particularly targeted by us to confirm their reported light curves and determine amplitudes and periods if a light curve was seen. Conversely, the 13 objects reported in this paper (Table 4) were selected because of their size and brightness, and not because of previous reports of their variability.

In comparison with the percentages of KBOs with large-amplitude light curves (>0.40 mag, or about 1.5 difference in brightness), the four main-belt asteroids with $D > 400$ km have $f(\Delta m_R \geq 0.40) = 0/4$ (0%), the largest being only about 0.15 mag (Lagerkvist, Harris, & Zappalà 1989; Tedesco 1989). For main-belt asteroids with $D > 200$ km,

TABLE 11
Other KBOs with Reported Light-Curve Observations

Name	Class[a]	H (mag)	Δ mag	P (hr)	i (deg)	e	a (AU)	Refs.
(28978) Ixion 2001 KX$_{76}$	R	3.2	...	...	19.7	0.246	39.3	1, 2
(19308) 1996 TO$_{66}$	C	4.5	0.25	7.9	27.4	0.115	43.4	1, 3
(24835) 1995 SM$_{55}$	C	4.8	...	...	27.0	0.110	42.1	1
(15874) 1996 TL$_{66}$	S	5.4	...	...	23.9	0.587	84.9	4, 5
(26308) 1998 SM$_{165}$	C	5.8	0.45	7.1	13.5	0.371	47.8	1, 6
(15875) 1996 TP$_{66}$	R	6.8	...	...	5.7	0.336	39.7	4, 7
(15789) 1993 SC	R	6.9	...	...	5.2	0.185	39.6	4, 8
(15820) 1994 TB	R	7.1	...	...	12.1	0.321	39.7	1
(32929) 1995 QY$_9$	R	7.5	0.60	7.3	4.8	0.266	39.8	1, 4

[a] (S) Scattered-type object; (C) classical-type object; (R) resonance-type object.
References.—(1) Sheppard 2002; (2) Ortiz et al. 2001; (3) Hainaut et al. 2000; (4) Romanishin & Tegler 1999; (5) Luu & Jewitt 1998; (6) Romanishin et al. 2001.; (7) Collander-Brown et al. 1999; (8) Davies, McBride, & Green 1997

$f(\Delta m_R \geq 0.40) = 5/27$ (19%) when their pole orientations are $\theta = 90°$ to our line of sight. With an average pole orientation of $\theta = 60°$, only 11% [$f(\Delta m_R \geq 0.40) = 3/27$] would have large-amplitude light curves. These are thought to be the Jacobi ellipsoid–type objects. Asteroids with $D < 200$ km have $f(\Delta m_R \geq 0.40) = 111/482$ (23%), while the Centaurs [Chiron, Asbolus, Pholus, Chariklo, Hylonome, (31824) 1999 UG$_5$, and (32532) 2001 PT$_{13}$] have $f(\Delta m_R \geq 0.40) = 0/7$ (0%). Most of these objects are small and thus thought to be collisional fragments.

Figure 13 shows how the largest ($D > 200$ km) main-belt asteroids compare with the Kuiper belt objects. Many of the KBOs fall in the upper and upper-left parts of this figure, where the Jacobi ellipsoids are encountered in the asteroid belt. There is a bias in the KBO sample, since light variations of less than about 0.1 mag are very hard to detect, as are long single-peak periods over 24 hours.

Student's t-test was used to measure the significance of the differences between the means of the asteroid and KBO periods and amplitudes. In order to reduce the effects of observational bias, we used only periods less than 10 hr and amplitudes greater than 0.2 mag from Figure 13. We found that the period distributions of the asteroids are significantly shorter than for the KBOs. The mean periods are 5.56 ± 0.89 and 7.80 ± 1.20 hr for the asteroids and KBOs, respectively, giving a t-statistic of -3.84 (12 degrees of freedom), which is significant at the 99.7% confidence level. This difference is formally significant at the 3 σ level by Student's t-test, but it would be highly desirable to obtain more data from another large unbiased survey in order to be sure of the effect. The KBOs have a larger mean amplitude, but the significance between the difference of means, 0.36 ± 0.11 versus 0.50 ± 0.16 mag for the asteroids and KBOs, respectively, is only 95% (2 σ), with a t-statistic of -1.83. This may be because the KBOs are less dense and more elongated, on average, than asteroids. Below we discuss in more detail the shape distribution of the Kuiper belt.

5.2. Shape Distribution Models

What constraints can be placed on the intrinsic distribution of KBO shapes from the apparent (sky-plane projected) distribution? We used a Monte Carlo model to project several assumed intrinsic distributions into the plane of the sky and then compared them with the observations. This was done by using a pole orientation distribution proportional to sin θ. The apparent axis ratio for each object was then calculated from this pole orientation distribution and the intrinsic axis ratio selected from one of several assumed distributions.

First, as an extreme case, we ask whether the data are consistent with selection from intrinsic distributions in which all the objects have a single axis ratio $x = b/a$, with $x = 0.80, 0.66, 0.57$, or 0.50. Figure 14 shows that the form of the resulting amplitude distribution differs dramatically from what is observed. We conclude that the distribution KBO light-curve amplitudes cannot be modeled as the result of projection on any single axis ratio. A range of shapes must be present. While not surprising, this result does serve to demonstrate that the KBO light-curve sample is of sufficient size to be diagnostic.

Secondly, we explored the effect of the width of the distribution using

$$\Psi(x)dx = \exp\left[\frac{-(x - x_0)^2}{2\sigma^2}\right]dx , \qquad (8)$$

where $\Psi(x)dx$ is the number of KBOs with axis ratios in the range x to $x + dx$, σ is the standard deviation or width parameter, and x_0 is the mean axis ratio. Examples for $x_0 = 0.66$ and $\sigma = 0$, 0.35, 0.75, and 1.0 are plotted in Figure 15. We assumed that all objects had axis ratios $0.5 \leq x \leq 1.0$. The figure shows that the data require an intrinsically broad distribution of body shapes, specifically with a dispersion comparable to the mean axis ratio.

Thirdly, we assumed that the axis ratios of the KBOs followed a differential power-law distribution of the form

$$\Psi(x)dx = x^{-q}\,dx , \qquad (9)$$

FIG. 13.—Rotational variability and periods of all the asteroids with diameters over 200 km and of Kuiper belt objects in our sample. Objects in the upper and upper-left portions of the graph are possibly rotationally deformed rubble piles. The asteroid amplitudes that were taken from pole orientations of 90° have been corrected to a mean pole orientation at 60° to better compare them with the KBOs of unknown orientation. KBOs with amplitudes ≤0.1 mag and periods ≥12 hr are subject to observational bias against detection.
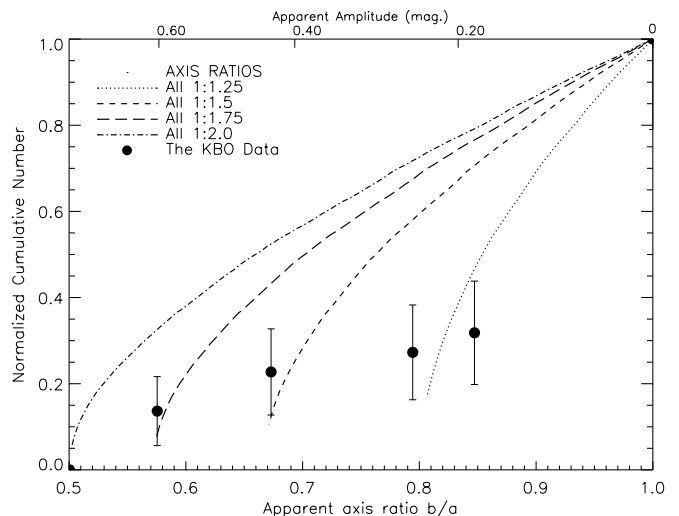

FIG. 14.—Monte Carlo simulations using a constant axis ratio for all KBOs. Error bars for the KBO points are based on a Poisson distribution.
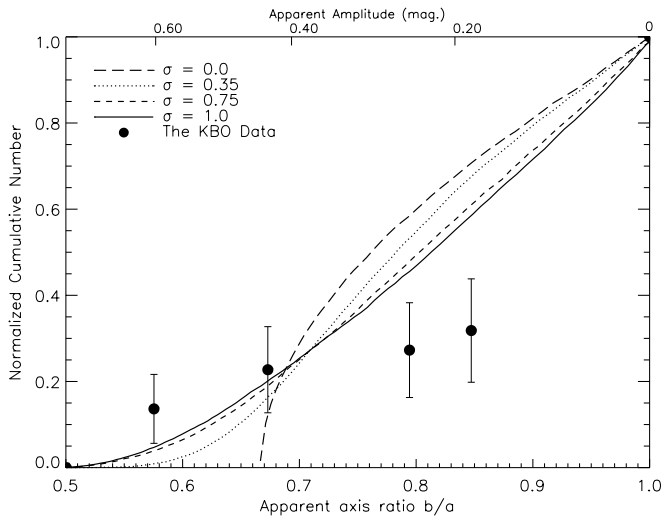
FIG. 15.—Monte Carlo simulations using Gaussians centered on the axis ratio of 1 : 1.5 with different standard deviations (eq. [8]). Error bars for the KBO points are based on a Poisson distribution.

where q is a constant and $\Psi(x)dx$ is again the number of KBOs with axis ratios in the range x to $x + dx$. We assumed $0.5 \leq x \leq 1.0$. The results can be seen in Figure 16. The $q = -5$ distribution is very similar to an exponential distribution, with its peak at an axis ratio of $x = 1$. Again we see that the models fit the data better with a broader distribution of axis ratios.

Fourth, we ask whether the data are consistent with selection from an intrinsic distribution of shapes caused by collisional fragmentation. The fragment shape distribution is taken from Catullo et al. (1984). Figure 17 shows that the KBO Δm distribution is inconsistent with the collisional fragment distribution in the sense that more highly elongated KBOs are found than would be expected from impact fragments. This finding is consistent with collisional models (Farinella & Davis 1996; Kenyon & Luu 1999) in the sense that only KBOs smaller than a critical diameter
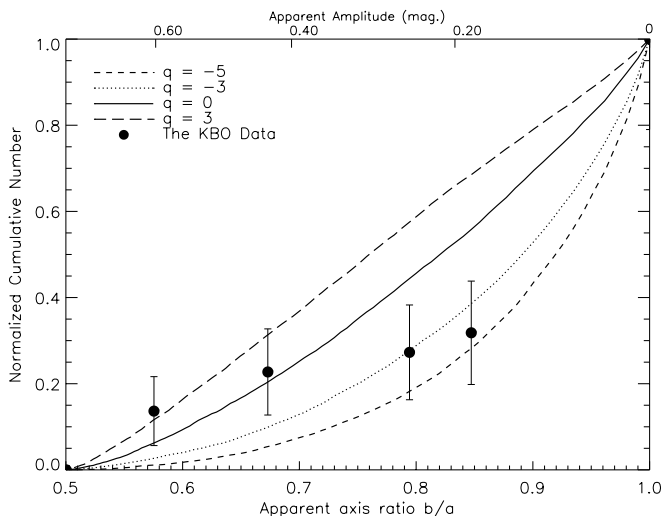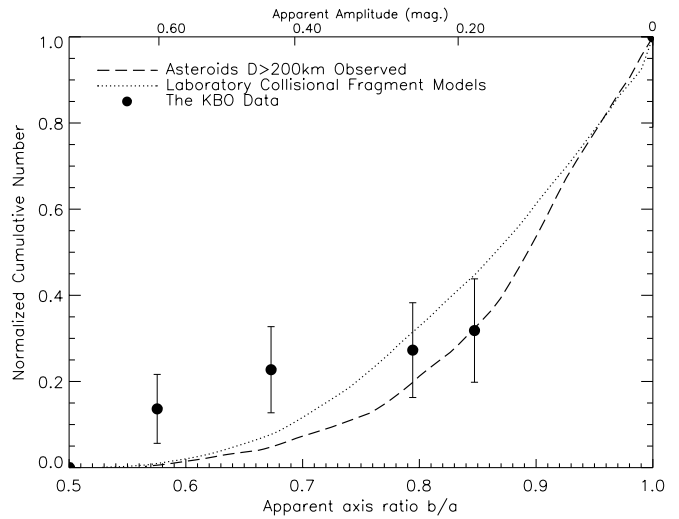
FIG. 17.—Same as Fig. 15, but using all large asteroids ($D > 200$ km) and a collisional distribution from Catullo et al. (1984).

~100 km are likely to be impact fragments, while the observed KBOs are all larger than this.

Finally, we ask whether the data are consistent with selection from an intrinsic distribution of shapes like that measured in the large ($D > 200$ km) main-belt asteroid population. We take this distribution from the published light-curve database of Lagerkvist et al. (1989), which has been updated by A. Harris on the World Wide Web.[1] The results are shown in Figure 17, where we see that the KBOs contain a larger fraction of highly elongated objects than is found among the main-belt asteroids. A plausible explanation for such a large fraction of the highly elongated KBOs is that the objects are very large yet structurally weak and of low density. This would allow many of the KBOs to be gravitationally bound rubble piles easily distorted by centripetal forces due to their rotation.

5.3. KBO Density Comparisons in the Solar System

The Kuiper belt objects are thought to consist of water ice with some rocky material mixed in, similar to the comets. How do the densities of the icy outer satellites compare with what we have found for our sample of KBOs? In Figure 18, we plot all the outer icy bodies in the solar system that have well-known densities and are less than 3000 km in diameter. There is a clear trend, with larger objects being denser. The KBOs seem to follow this trend. We also note there appears to be a trend with object size versus light-curve amplitude and size versus period for the KBOs in our data. Objects that have densities less than that of water ice (1000 kg m^{-3}) must have significant internal porosity or be composed of ices less dense than water (see Jewitt & Sheppard 2002).

To date, only about 10 main-belt asteroids have reliably measured bulk densities. Most of these are from perturbation calculations between asteroids, though two have been measured by passing spacecraft and a few others found from the orbital motions of known companions. Most asteroid densities are consistent with that of rock, 2000 kg m$^{-3} \leq \rho \leq 3000$ kg m^{-3}. Some of the asteroid densities have

FIG. 16.—Same as Fig. 15, but using power laws of different slopes (eq. [9]).

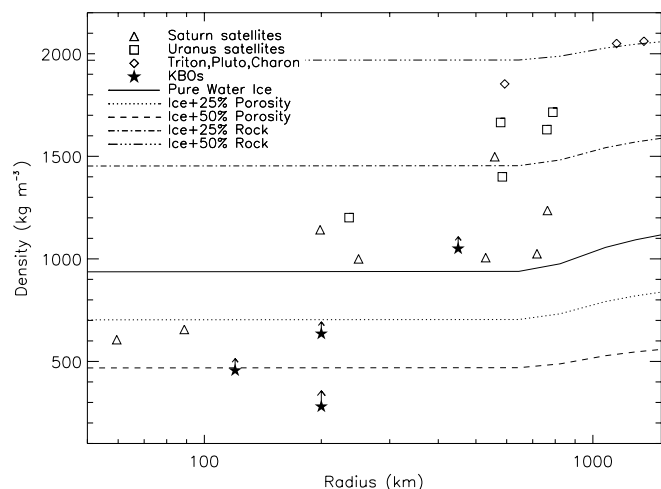[1] At http://cfa-www.harvard.edu/iau/lists/LightcurveDat.html.

FIG. 18.—Sizes and densities of icy bodies. A trend is observed in which the larger the object, the higher the density. The solid line is overplotted to show the expected bulk density of a pure water ice sphere with size (Lupo & Lewis 1979). Other lines indicate how the density would behave with added porosity and rock. Data points for satellite densities are from the JPL Solar System Dynamics Web page.

been found to be lower than expected and attributed to internal porosity, possibly from rubble-pile structure (Yeomans et al. 1997).

In Table 9, we present new densities for five main-belt asteroids calculated under the assumption that they are equilibrium rotational (Jacobi ellipsoid) figures. We used their light curves as seen at maximum amplitude, to eliminate the effects of projection. The densities are higher than those of the KBOs obtained using the same method (Fig. 19) but lower than expected for solid-rock objects. This provides another hint that these objects may be internally porous. The densities of 15 Eunomia (790 ± 210 kg m^{-3}) and 16 Psyche (1800 ± 600 kg m^{-3}) were reported separately from measurements of gravitational perturbations (Hilton 1997; Viateau 2000). The higher density for 16 Psyche is particularly interesting because this object is an M-type asteroid and thus expected to have a high density.
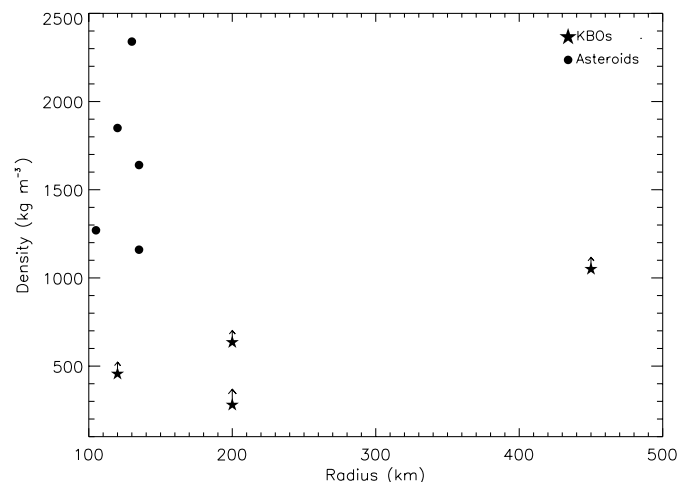

FIG. 19.—Sizes and densities of possible rotationally deformed KBOs and main-belt asteroids. The asteroids have lower densities than expected for solid rock but are still denser than the KBOs.

The main-belt asteroid 45 Eugenia was found to have a companion, which was used by Merline et al. (1999) to find a density of 1200^{+600}_{-200} kg m^{-3}. Asteroid densities found by others are probably underestimated, since they assumed that the objects were spheres. A sphere has the highest volume–to–projected area ratio, and thus any deviation from a sphere will cause the object to appear to have a lower density. We calculated the density for these objects using the assumption they are Jacobi ellipsoids, and thus the parameters used are the well-known period and amplitude from the light curves. Interestingly, the five best examples of main-belt rotationally deformed asteroids (Table 9) are found in all the main classes, two C-type, and one each of S, P, and M types.

6. PHASE FUNCTIONS OF KBOs

At large phase angles, the phase function in equation (1) may be approximated as

$$\phi(\alpha) = 10^{-\beta\alpha} , \qquad (10)$$

where α is the phase angle in degrees and β is the "linear" phase coefficient. Empirically, the magnitude of β is inversely correlated with the surface albedo (Gehrels 1970; Bowell et al. 1989; Belskaya & Shevchenko 2000), suggesting that we might be able to indirectly assess the albedos of KBOs from their phase functions. Unfortunately, this is not possible. The maximum phase angle attained by an object at distance R (AU) is roughly $\alpha_{\max} = 180/(\pi R)$. At $R = 30$ AU, for instance, $\alpha_{\max} = 1°9$. This is exactly the phase-angle range in which the opposition surge is potentially important (Scaltriti & Zappalà 1980; Belskaya & Shevchenko 2000). The opposition surge is a complex, multiple-scattering phenomenon that occurs in the grains of a porous regolith. The magnitude of the opposition surge, which causes an increase in scattered intensity over and above that predicted by equation (10) at small α, is determined by coherent backscattering and is a complex function of regolith physical and optical properties. It is not simply related to the albedo, and equation (10) must be modified to take account of this surge. Nevertheless, the phase functions provide a new basis for comparison of the KBOs and should be measured if we are to accurately assess the sizes of KBOs from their optical data.

Seven of the KBOs were observed over a range of phase angles sufficient for us to measure the phase darkening. We plot the quantity $m_R(1, 1, \alpha) = m_R - 5 \log R\Delta$ against α for these seven KBOs in Figures 20 and 21. When observations from consecutive nights were available, we averaged the phase angle and apparent magnitude over those nights to create a single point with small uncertainty. If an object showed a light curve, its time-averaged mean apparent magnitude was used. The linear least-squares fits to the KBO data are listed in Table 12 and shown in Figure 20. Within the uncertainties, we find that photometry of the seven KBOs is compatible with $\beta(\alpha < 2°) = 0.15 \pm 0.01$ mag deg^{-1}. In contrast, the phase function for Pluto was found to be linear throughout the 0° to 2° phase-angle range with $\beta(\alpha < 2°) = 0.0372 \pm 0.0016$ mag deg^{-1}, indicating a very shallow, if any, opposition surge and consistent with a high-albedo surface (Tholen & Tedesco 1994).

Since the observations at small phase angle are affected by the opposition surge, caused by multiple scattering
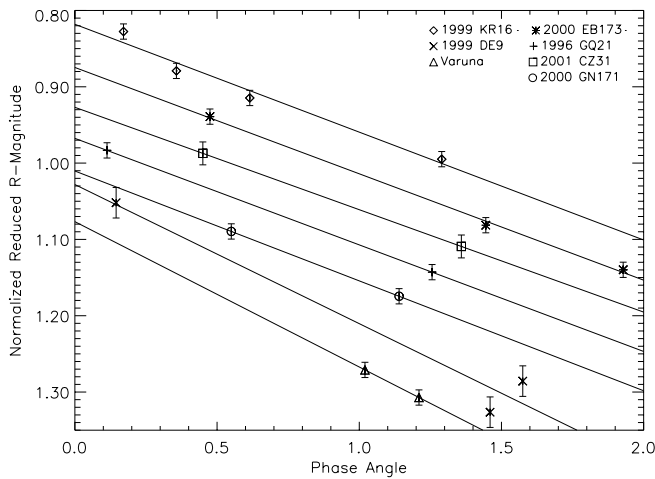
FIG. 20.—Phase functions for KBOs observed at several phase angles. The average linear fit gives a phase coefficient of $\beta(\alpha < 2°) = 0.15$ mag deg^{-1}. Objects with more than two data points show evidence of the nonlinear opposition surge.

within the porous regolith, we also fitted the data using the Bowell et al. (1989) H-G scattering parameterization. This technique yields a curved relation at small phase angles that becomes asymptotically like the linear β-relation at large phase angles and thus attempts to account for the opposition surge. In the Bowell et al. formalism, H is the absolute magnitude of the object, analogous to $m_R(1, 1, 0)$. The parameter G provides a measure of the slope of the phase function at large angles, analogous to β. It is scaled so that $G = 0$ corresponds to the darkest surfaces found on the asteroids, while $G = 1$ corresponds to the brightest (Bowell et al. 1989). The results of the H-G fits are presented in Table 12 and Figures 21 and 22. The KBOs show steep slopes with a possible moderate opposition surge. The best-fit values of the G-parameter are very low, with an average of -0.21. This small G-value more closely resembles that of dark, C-type asteroids ($G \sim 0.15$) than the brighter S-types

($G \sim 0.25$) in the main belt. This is consistent with, though does not prove, the assumption that the majority of KBOs are of very low albedo. The similarity of the slopes of the phase functions of all KBOs in our sample suggests comparative uniformity of the surface compositions, physical states, and albedos. As a comparison, Pluto was found to have a best-fit $G = 0.88 \pm 0.02$ using data from Tholen & Tedesco (1994). The dramatic difference between the back-scattering phase functions of Pluto and the smaller KBOs studied here is shown in Figure 22. This difference is again consistent with the smaller KBOs having low-albedo (0.04?) surfaces qualitatively different from the high-albedo (0.6), ice-covered surface of Pluto.

7. SUMMARY

We have conducted a systematic program to assess the rotations and sky-plane shapes of Kuiper belt objects from their optical light curves.

1. Four of 13 (31%) bright KBOs in our sample [(33128) 1998 BU$_{48}$, 2000 GN$_{171}$, (20000) Varuna, and (40314) 1999 KR$_{16}$] show light curves with range $\Delta m \geq 0.15$ mag. In an

TABLE 12
PHASE FUNCTION DATA FOR KBOs

Name	H	G	$\beta(\alpha < 2°)^{a}$
2000 EB$_{173}$	4.44 ± 0.02	-0.15 ± 0.05	0.14 ± 0.02
Varuna............	3.21 ± 0.05	-0.58 ± 0.10	0.19 ± 0.06
1999 DE$_{9}$........	4.53 ± 0.03	-0.44 ± 0.07	0.18 ± 0.06
1996 GQ$_{21}$.......	4.47 ± 0.02	-0.04 ± 0.05	0.14 ± 0.03
2000 GN$_{171}$	5.98 ± 0.02	-0.12 ± 0.05	0.14 ± 0.03
1999 KR$_{16}$.......	5.37 ± 0.02	-0.08 ± 0.05	0.14 ± 0.02
2001 CZ$_{31}$........	5.53 ± 0.03	-0.05 ± 0.07	0.13 ± 0.04
Mean...........	...	-0.21 ± 0.04	0.15 ± 0.01
Pluto^{b}..........	-1.00 ± 0.01	0.88 ± 0.02	0.0372 ± 0.0016

^{a} The phase coefficient at phase angles less than $2°$.
^{b} Data for Pluto are from Tholen & Tedesco 1994, while the G-value was calculated by us.
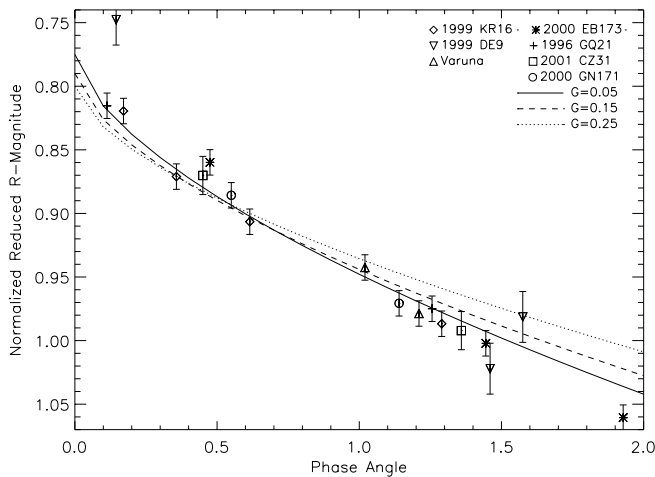

FIG. 21.—Phase functions of all seven KBOs observed at multiple phase angles. The reduced magnitudes have been normalized to show all objects relative slopes. Overplotted are fits of the slope parameter $G = 0.05$, 0.15 (C-type), and 0.25 (S-type). The best-fit slope parameters of all KBOs are below $G = 0.05$, which is consistent with scattering from low-albedo surfaces.
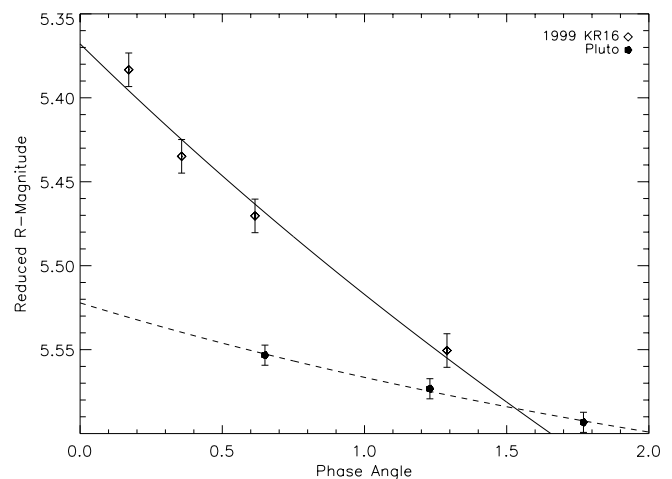

FIG. 22.—Comparison of phase functions for the typical KBO 1999 KR$_{16}$ and Pluto. The solid line is the best-fit Bowell et al. (1989) H-G phase function for (40314) 1999 KR$_{16}$, with $G = -0.08$. Data points for Pluto are from Tholen & Tedesco (1994) and are offset in the vertical direction from reduced magnitude -1.0. Pluto has a best-fit $G = 0.88$ (*dashed line*).

enlarged sample combining objects from the present work with objects from the literature, seven of 22 (32%) objects have $\Delta m \geq 0.15$ mag.

2. The fraction of KBOs with $\Delta m \geq 0.4$ mag (23%) exceeds the corresponding fraction in the main-belt asteroids (11%) by a factor of 2. The KBO Δm distribution is inconsistent with the distribution of impact fragment shapes reported by Catullo et al. (1984).

3. The large KBOs (33128) 1998 BU_{48}, 2000 GN_{171}, and (20000) Varuna show large periodic variability with photometric ranges 0.68 ± 0.04, 0.61 ± 0.03, and 0.45 ± 0.03 mag, respectively, and short double-peaked periods of 9.8 ± 0.1, 8.329 ± 0.005, and 6.3565 ± 0.0002 hr, respectively. Their $BVRI$ colors are invariant with respect to rotational phase at the few-percent level of accuracy.

4. If these objects are equilibrium rubble piles distorted by centripetal forces due to their own rotation, the implied densities must be comparable to or less than that of water.

Such low densities may be naturally explained if the KBOs are internally porous.

5. In the phase-angle range $0° \leq \alpha \leq 2°$, the average slope of the phase function of seven KBOs is $\beta(\alpha < 2°) = 0.15 \pm 0.01$ mag deg^{-1} (equivalently, $G = -0.2$). The corresponding slope for ice-covered Pluto is $\beta(\alpha < 2°) \approx 0.04$ mag deg^{-1} (equivalently, $G = 0.88$). The large difference is caused by pronounced opposition brightening of the KBOs, strongly suggesting that they possess porous, low-albedo surfaces unlike that of ice-covered Pluto.

REFERENCES

Asphaug, E., Ostro, S. J., Hudson, R. S., Scheeres, D. J., & Benz, W. 1998, Nature, 393, 437
Belskaya, I. N., & Shevchenko, V. G. 2000, Icarus, 147, 94
Binzel, R. P., Farinella, P., Zappalà, V., & Cellino, A. 1989, in Asteroids II, ed. R. P. Binzel, T. Gehrels, & M. S. Matthews (Tucson: Univ. Arizona Press), 416
Boehnhardt, H., et al. 2001, A&A, 378, 653
Bowell, E., Hapke, B., Domingue, D., Lumme, K., Peltoniemi, J., & Harris, A. W. 1989, in Asteroids II, ed. R. P. Binzel, T. Gehrels, & M. S. Matthews (Tucson: Univ. Arizona Press), 524
Brown, R. H., Cruikshank, D. P., & Pendleton, Y. 1999, ApJ, 519, L101
Burns, J. A., & Safronov, V. S. 1973, MNRAS, 165, 403
Capaccioni, F., et al. 1984, Nature, 308, 832
Catullo, V., Zappalà, V., Farinella, P., & Paolicchi, P. 1984, A&A, 138, 464
Chandrasekhar, S. 1987, Ellipsoidal Figures of Equilibrium (New York: Dover)
Collander-Brown, S. J., Fitzsimmons, A., Fletcher, E., Irwin, M. J., & Williams, I. P. 1999, MNRAS, 308, 588
Davies, J. K., McBride, N., & Green, S. F. 1997, Icarus, 125, 61
Davis, D. R., & Farinella, P. 1997, Icarus, 125, 50
De Angelis, G. 1995, Planet. Space Sci., 43, 649
Degewij, J., Tedesco, E. F., & Zellner, B. 1979, Icarus, 40, 364
Drummond, J. D., Weidenschilling, S. J., Chapman, C. R., & Davis, D. R. 1991, Icarus, 89, 44
Duncan, M., Quinn, T., & Tremaine, S. 1988, ApJ, 328, L69
Durda, D. D., & Stern, S. A. 2000, Icarus, 145, 220
Farinella, P., & Davis, D. R. 1996, Science, 273, 938
Farinella, P., Paolicchi, P., Tedesco, E. F., & Zappalà, V. 1981, Icarus, 46, 114
Farinella, P., Paolicchi, P., & Zappalà, V. 1982, Icarus, 52, 409
Farnham, T. L. 2001, IAU Circ. 7583
Fernández, J. A. 1980, MNRAS, 192, 481
Fujiwara, A., Kamimoto, G., & Tsukamoto, A. 1978, Nature, 272, 602
Gehrels, T. 1970, in Surfaces and Interiors of Planets and Satellites, ed. A. Dollfus (London: Academic), 355
Green, S. F., McBride, N., Ó Ceallaigh, D. P., Fitzsimmons, A., Williams, I. P., & Irwin, M. J. 1997, MNRAS, 290, 186
Hainaut, O. R., et al. 2000, A&A, 356, 1076
Harris, A. W. 1994, Icarus, 107, 209
Hilton, J. L. 1997, AJ, 114, 402
Jewitt, D., & Luu, J. 1993, Nature, 362, 730
Jewitt, D., Luu, J., & Chen, J. 1996, AJ, 112, 1225
Jewitt, D. C., & Luu, J. X. 2001, AJ, 122, 2099
Jewitt, D. C., & Sheppard, S. S. 2002, AJ, 123, 2110
Kenyon, S. J., & Luu, J. X. 1999, AJ, 118, 1101
Lagerkvist, C.-I., Harris, A. W., & Zappalà, V. 1989, in Asteroids II, ed. R. P. Binzel, T. Gehrels, & M. S. Matthews (Tucson: Univ. Arizona Press), 1162
Landolt, A. U. 1992, AJ, 104, 340
Leinhardt, Z. M., Richardson, D. C., & Quinn, T. 2000, Icarus, 146, 133
Lupo, M. J., & Lewis, J. S. 1979, Icarus, 40, 157
Luu, J., & Jewitt, D. 1996, AJ, 112, 2310
Luu, J. X., & Jewitt, D. C. 1998, ApJ, 494, L117
Merline, W. J., et al. 1999, Nature, 401, 565
Ortiz, J. L., López-Moreno, J. J., Gutiérrez, P. J., & Baumont, S. 2001, BAAS, 33, 1047
Romanishin, W., & Tegler, S. C. 1999, Nature, 398, 129
Romanishin, W., Tegler, S. C., Rettig, T. W., Consolmagno, G., & Botthof, B. 2001, Proc. Natl. Acad. Sci., 98, 11863
Ryan, E. V., Davis, D. R., & Giblin, I. 1999, Icarus, 142, 56
Scaltriti, F., & Zappalà, V. 1980, A&A, 83, 249
Sekiguchi, T., Boehnhardt, H., Hainaut, O. R., & Delahodde, C. E. 2002, A&A, 385, 281
Sheppard, S. S. 2002, in preparation
Stellingwerf, R. F. 1978, ApJ, 224, 953
Tedesco, E. F. 1989, in Asteroids II, ed. R. P. Binzel, T. Gehrels, & M. S. Matthews (Tucson: Univ. Arizona Press), 1090
Tegler, S. C., & Romanishin, W. 2000, Nature, 407, 979
Tholen, D. J. & Tedesco, E. F. 1994, Icarus, 108, 200
Viateau, B. 2000, A&A, 354, 725
Yeomans, D. K., et al. 1997, Science, 278, 2106